공학박사 학위논문

# Enhancement of Mechanical properties of Ti by Three-roll planetary rolling and Equal-channel angular pressing at low Temperature

## 저온 유성압연 및 등통로각 압축을 통한 순수 티타늄의 기계적 물성 증진

**2014 년 02 월**


**서울대학교 대학원**

**재료공학부**

**LI YUANLONG**

# Abstract

## Enhancement of Mechanical properties of Ti by Three-roll planetary rolling and Equal-channel angular pressing at low Temperature

**LI YUANLONG**

**Materials Science and Engineering**

**Seoul National University**

During the last decade, getting ultrafine-grained (UFG) in pure metals or alloys is the main purpose to obtain superior mechanical properties according to the Hall-Petch relationship between grain size and yield strength. Severe plastic deformation (SPD) process is one of the processing to get UFG structure materials even hard to deform materials such as titanium and its alloys. This thesis examined recent developments related to the use of three roll planetary rolling (PSW) and equal channel angular pressing (ECAP) processes for grain refinement including modifying conventional method of these two process to increase the process efficiency and techniques for up-scaling the procedure and for the processing of hard-to-deform materials. Commercially pure (CP) titanium grade 2 and 4 was chosen to be work material due to their superior mechanical

properties and biocompatibility in this study. Many efforts have been studied on improving mechanical properties on CP titanium. Nevertheless, it was always the main issue to sacrifice some part of the processing parameters such as temperature or deformation ratio due to the structural limit of HCP structure. In the present study the CP titanium was deformed by optimized low temperatures and effective deformation through the upgraded processing of two methods. After these optimized condition the deformed materials had extremely high values of yield strength and tensile strength close to record literature values of these titanium grades and matching, or even surpassing, the levels for conventional Ti-6Al-4V alloy were obtained by getting UFG grain structure. Furthermore, computer based simulation also conducted and compared with real experimental results in order to understand the mechanisms by using SFTC DEFROM-3D software although it is insufficient on explaining whole process.

---

***Keywords*: Ultra-fine grain, Titanium (Ti), Three roll planetary rolling (PWS), Equal channel angular pressing (ECAP), Severe plastic deformation (SPD), Mechanical properties.**

# Contents

# List of Tables

# List of Figures

# Chapter Ⅰ.

# Enhancement of mechanical properties of titanium by three roll planetary rolling

# 1. Introduction

## 1.1 Back ground of three roll planetary rolling

Three-roll planetary rolling is one of the high efficient rolling processes that can produce most of the metals and its alloys to deform. The first equipment of this processing was invented in 1970s by SMS SIEMAG Company in Germany and later Switzerland and Japan also developed this kind of processing equipment. This process mainly produces on bar or tube structure of carbon steel, spring steel, Co-Cr alloy and pure titanium and its alloys and so on. Furthermore, because of fast process and economic concern it has been extensively used in manufacturing industry area[1].

A three roll planetary rolling mill consists of a set of planetary transmission gears and three rollers separated with equal angle. The three rollers are so located that they have an offset angle α with respect to the vertical plane and inclined angle β with respect to the central symmetrical axis, as shown in Fig. 1. Where, the offset angle α decides reduction ratio, the bigger the higher. The inclined angle β is proportional to the compression efficiency and speed of the processing materials. Usually, when angle of α increases it needs higher press due to the large contact area. In zero degree of β there

will be no deformation because the material may turn in the place without moving horizontally[2].

Three-roll planetary rolling is also called PSW[2] (Planetensh rägwalzwerk) or HRM (High Reduction Machine) due to the reduction of cross-sectional area. Accordingly, the production line of the factory can be shortened considerably. In some factories, some kind of special metal (or its alloys) rod and tubes are manufactured by three roll planetary rolling mills for some merits, such as lower rolling force, lower cost, lower power, lower lateral extension, and high process speed, etc.

A three-roll planetary rolling mill is also one of the efficient methods of SPD process to get UFG structures. In this paper UFG structured CP Ti grade 2 and grade 4 rods were fabricated by three roll planetary rolling process.

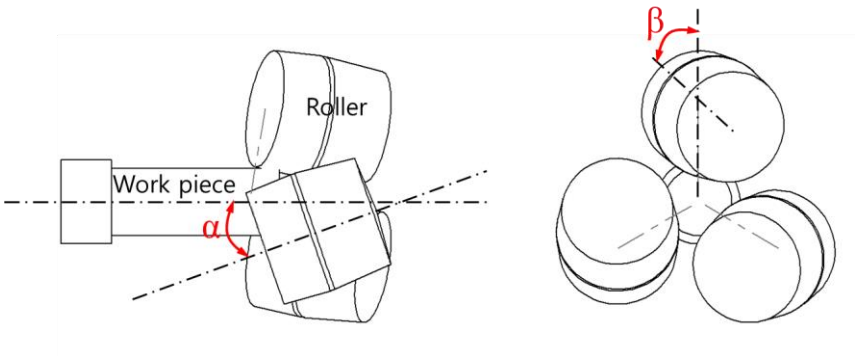


Fig. 1. Schematic diagram of three roll planetary rolling process with the offset angle of α and inclined angle of β.

## 1.2 Principals of three roll planetary rolling

The principal arrangement of a planetary rolling mill comprises three rolls arranged around the outside of the sample and cylindrical mandrel located inside and fixed in position by axially adjustable clamping devices[1].

The rolling process is characterized in that the three tapered rolls arranged in a planetary gearbox move transversely to the longitudinal axis in the direction of the work piece circumference. During the forming, the rolls surround only about 30% of the work piece, causing a significant deformation of the work piece into a non-circular shape known as ‘triangulation’ before, in the final forming section, a round bar is produced. Fig. 2 illustrates the materials deformation in the various areas.

Since all of the three rolls are inclined same angle of β the partial velocity of the deformation is $V \cdot \sin\beta$, where V is revolution per minute (RPM) of the three rolls. Whilst friction force is the only driving force to move forward the materials automatically and the distance between those three rolls can make possible the final dimension of the materials. During the process materials are not only pass through horizontally but also rotate to central symmetrical axis as called spiral movement.

Three-roll planetary rolling is famous as high efficiency and reduction ratio since it has been invented. Furthermore, this process has many advantages concerning as below[3-5].

1) No need any extra force and guide to pass through the rolls. Three-roll planetary rolling can pass the materials automatically without of any back force, but only in the beginning. During the process the equipment has relatively lower pressure to produce materials with constant speed and stress.
2) It can improve the physical and mechanical properties of the materials. Three-roll planetary rolling can decrease the inside pores and cracks of the materials, so that it improves the density and the crack propagation of the materials after processing. Processed materials have no micro-crack and surface defect, and have low tolerance value of $\pm$ 1%. Although the surface of the processed materials has some spiral tracks, it is negligible because it does not influence further treatment on the materials and has no effect on the final products.
3) It saves energy. Due to the huge deformation on the materials by friction force that transfer to a heat energy there is no

much heat loss even make extra increment in original temperature. Therefore, it make possible to decrease the processing temperature even at room temperature in soft materials. In this regards, this process at list save 20% of energies compare to other technics.

4) It has low cost on processing. The equipment of three-roll planetary rolling has very simple structure and light compare to other heavy rolling machine. Therefore, it has low cost of construction and producing the materials. So, this process not only takes center stage in major and minor enterprisers, but also in research area to make new kinds of materials.

Although three-roll planetary rolling has many advantages, it also has some disadvantages compare to other process as below.

1) It is hard to produce small diameter of materials. Reduction efficient would decrease a lot when produce small dimension of materials.

2) The rolls are easy wear and tear. The area of the roll that decrease diameter is very small and after many times of rolling rolls would change shape.

3) Spiral tracks occur on the surface. Due to its special work process spiral tracks will occur on the surface and sometimes

influences the quality of the final products. The reasons that may cause the problem are processing temperature, friction force between roll and materials and reduction ratios.

4) Sometimes the materials would be stuck in the rollers. The trapping status usually happens in hard deformable materials due to their strong strength. Hard to deform materials need a rapid increment of pressing force between the rollers in a very short time, however, the punching process will break down because of the concave structure in the fore part that causes less friction force between material and rollers and less friction force will slow down the speed of the processing in which the temperature of the material could decrease rapidly. So, the materials are more difficulty to deform. However, this problem can simply solve by machining head of the materials to avoid trapping between the rollers.

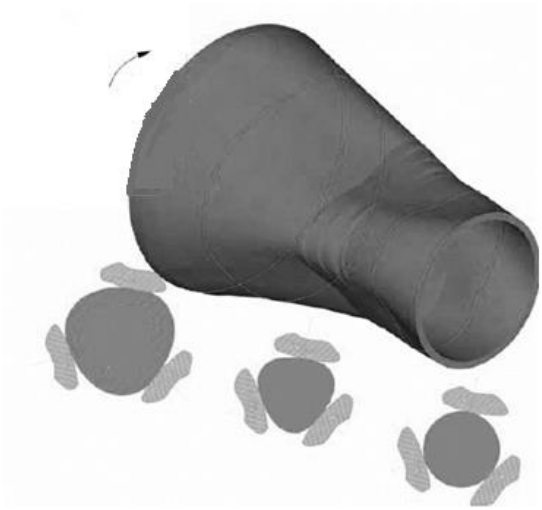

Fig. 2. Schematic diagram of shape variation on work piece during the PSW deformation where sample change its shape from round to ‘triangulation’ and finally round shape again.

## 2. Experiment and results

### 2.1 Materials and method

In this study commercial purity (CP) titanium grade 2 (ASTM B348.09 Korea) and grade 4 (ASTM B348-99 Japan) were chosen as processing materials. The as received chemical composition and the mechanical properties of these two materials are listed in Table 1. Diameter of 25 mm with length of 150 mm extruded rods was used in this experiment both in grade 2 and grade 4 CP titanium. The chemical composition of those materials is listed in Table 1. Fig. 3 and Fig. 4 illustrate the microstructure of these materials that have an average grain size of 20 μm and 15 μm, respectively. The grain orientation of those materials are prismatic plane <10-10> and <2-1-10> which is normal texture structure in extrude materials. As received CP titanium grade 2 has 278 MPa, 378 MPa of yield strength and ultimate tensile strength (UTS) and elongation to break is 36.7%. While, grade 4 has 600 MPa, 750 MPa of yield strength and UTS and elongation of 16.8%.

In this paper CP titanium grade 2 and 4 bars were decreased diameter up to 64% step by step. In which, each step has reduced about 20% of cross-sectional area. This process has also investigated

at different temperatures of 300°C, 350°C, 400°C and 450°C in order to receive the optimized processing condition. After processing each sample were polished and observed by electron backscatter diffraction (EBSD) analysis to get microstructure characteristics.

Table 1. Chemical composition and mechanical properties of as-received grade 2 and grade 4 CP Ti by supplier and measurements.

| Grade | Chemical composition (max wt%) | | | | | Mechanical properties | | |
|---|---|---|---|---|---|---|---|---|
| | C | O | N | H | Fe | $\sigma_{YS}$ | $\sigma_{UTS}$ | ε % |
| Gr 2 | 0.08 | 0.25 | 0.03 | 0.015 | 0.3 | 350 MPa | 380 MPa | 27 |
| Gr 4 | 0.08 | 0.4 | 0.05 | 0.015 | 0.5 | 680 MPa | 750 MPa | 22 |

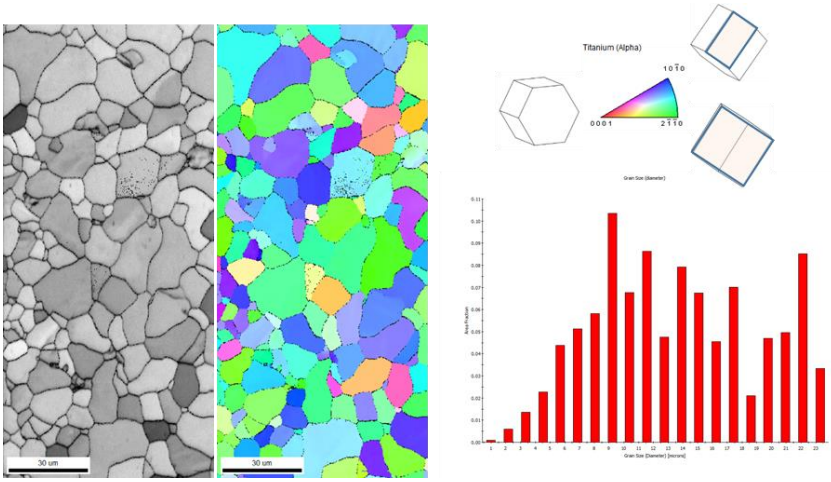


Fig. 3. Microstructure of as-received 25Φ grade 2 CP Ti with the initial texture formation by EBSD analysis. The most of grain size distribution is at a range of 10 ~ 27 μm while the average grain size calculated from linear intercept method is about 25 μm. In addition, most of the grain oriented in <1 0 0> and <2 -1 0> direction.

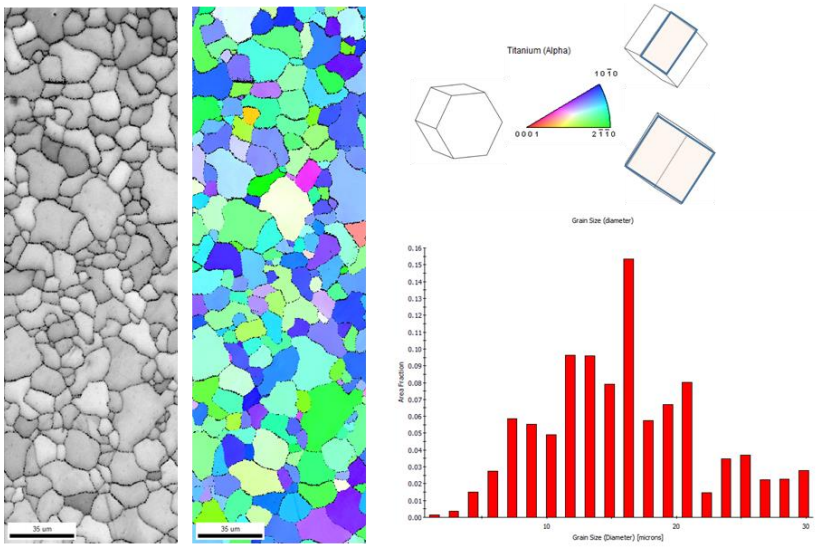


Fig. 4. Microstructure of as-received 30Φ grade 4 CP Ti with the initial texture formation by EBSD analysis. The most of the grain size distribution is at a range of 10 ~ 20 μm while the average grain size calculated from linear intercept method is about 16 μm. The texture formation as same as grade 2 CP Ti.

## 2.2 Experimental procedures

Both surface cleaned CP titanium grade 2 and 4 were heat treated in furnace 20 min using above temperatures. After heat treatment the titanium rod was milled from 25 to 22 mm of diameter (22.6% of cross-area reduction). Milled rod was quenched in the water to avoid grain growth. Water-cooled titanium rod was heat treated again in the same temperature and time, then milled from 22 to 20 mm of diameter (17.3% of cross-area reduction). After second rolling, the sample was quenched again. After two times of rolling the keeping time of the heat treatment was decreased to 10min at same temperature because of concerning of grain growth. After 10 min heat treatment sample milled again to 17 mm of diameter (27.8% of cross-area reduction) then did same cooling method as same as before. Again, the cooled titanium rod was heat-treated 10 min in the furnace and milled with final diameter of 15 mm (22.1% of cross-area reduction) then water quenched.

Before having a tensile test hardness measurement carried out in order to investigate the tendency of the sample's mechanical properties briefly due to easy observation and a correlation between hardness and strength. Hardness of the polished sample was investigated by Vickers hardness measurement method (ASTM E 92).

The Vickers hardness test method (Fig. 5) consists of indenting the sample with a sharp diamond indenter that has a right pyramid squared base.

In this study applied for 1 kg load to survey the hardness. The full load was maintained for 15 seconds for each clearly polished specimen. Then the two diagonals of the indentation left on the surface were measured by a microscope, after removal of the load, and calculate the average of them. The Vickers hardness was evaluated from the formula that is shown in below, when the mean diagonal of the indentation has been determined.

$$\text{Vickers hardness; } H_v = \frac{1.854 \times 9.807 \times F}{D^2} \text{ (MPa)}$$

Where: F= Load in kg;

D= Arithmetic mean of the two diagonals, $d_1$ and $d_2$ in mm.

Tensile test was conducted with a gauge length of 20mm, a thickness of 2mm and with of 4.85mm that cut from the milled rod titanium according to the ASTM E08 standard. In order to modify the strength on a different area of the sample, treated sample was cut to 5 pieces of longitudinal direction as shown Fig. 6 Each of the sample were marked number of 1, 2, 3, 4 and 5, in which 1 and 5 are

from rim part of the processed sample then 2 and 4 are middle part of the sample, 3 is the center part of the milled sample. All tensile tests were carried out at room temperature on an Instron 5586 universal testing machine using a crosshead velocity of 2mm/min. Metallographic specimens were ground with SiC paper up to 4000 grit, followed by 50% of colloidal silica suspension with 50% of hydrogen peroxide solution and polished mirror-like plane. Microstructures were observed on cross-sectional to the pressing direction by EBSD using a Hitachi SU70 field emission scanning electron microscope (FE-SEM).

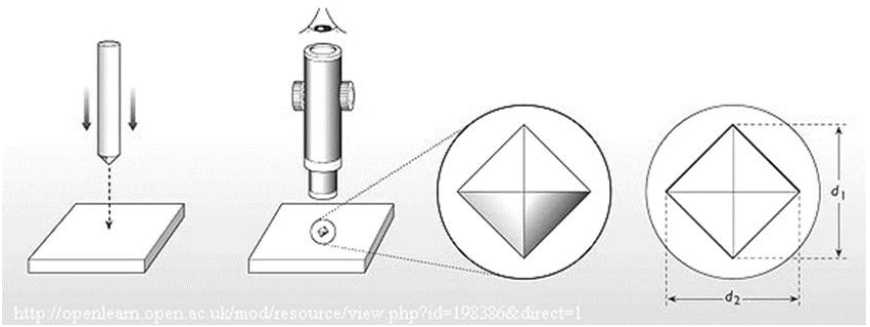


Fig. 5. Schematic diagram for Vickers hardness measurement method.

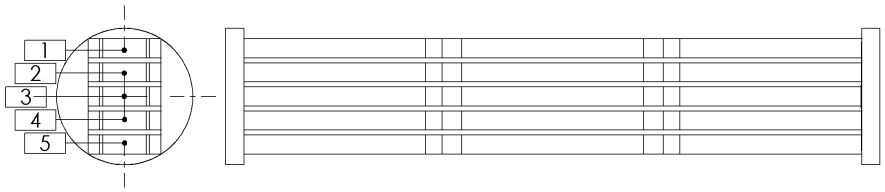


Fig. 6. Designated tensile specimen by ASTM standard specification where 1 and 5 belongs rim, 2 and 4 belongs middle and 3 belongs center (axis point), respectively.

## 2.3 Results and discussion

### 2.3.1 Microstructure observations

Unfortunately, at temperature of 300˚C both titanium grade 2 and 4 could not pass through the rollers and even slip occurred during the process due to of high stress necessity and low friction between rolls and material at low temperature. Fig. 7 shows the microstructure of after 4 passed grade 2 titanium at a processing temperature of 350˚C. Rim and middle part of the grain showed quite fine structure, however the grains in center still remained coarse structure which means that in this processing temperature, microstructure evolution is not efficient enough to do grain refinement in entire sample. The microstructure of 4 passed grade 2 titanium is shown in Fig. 8 that pressed at temperature of 400˚C. The grains located in center are almost the same as before at processing temperature of 350˚C. In addition, the mechanical properties of these two temperatures processed samples showed abnormal tendency that the ultimate tensile strength was decreased when further rolling was conducted after second rolling which means microcrack may occur during the process at low temperature due to not enough of absorption on strain energy by limited dislocation movements. Eventually, the

microstructure that processed at 450°C had fairly homogeneous distribution (see Fig. 11) in whole processed sample and showed promising improvement on mechanical properties. Because grain refinement by severe plastic deformation is strongly depending on processing temperature the lower the best improvement on mechanical properties 450°C could be the optimized temperature. In this consideration, grade 4 titanium was directly processed at temperature of 450°C depending on experience of processing grade 2 titanium. Thus, all explanation in this study will focus on optimized processing condition from now on.

Fig. 9 shows the microstructure of one pass CP titanium grade 2. As expected, the rim part has smallest grains due to the high deformation by screw force or shear stress, while the middle part of the grains begins doing grain refinement. Most of the grains in center part almost kept the same size like as received condition, however many twinning effect occurred in the coarse grains that also may increase the strength too[6, 7]. Fig. 10 also shows the 2 passed microstructure of the titanium. Same as before the grains remained almost same size in rim part, but middle and center part of the grains begin under a refinement process. After 4 passes of rolling whole part of grain become a fine grain structure even at center of the

sample as shown in Fig. 11. The graph in Fig. 12 illustrates the grain changes during the rolling process. Compare to the as received materials at final product the grain size decreased from 16 μm to at an average size of 0.75 μm that have a good agreement with similar work in the literature at this temperature range[8, 9] Fine grain structure would provide the materials strength by following section.

Microstructure of the 1 passed grade 4 titanium is shown in Fig. 13. In the first pressing grade 4 titanium also showed same trend of microstructure distribution compared with the grade 2 titanium. 2 and 4 times passed grade 4 Ti also showed same microstructure tendency comparing with grade 2 as same as before as shown in Fig. 14 and Fig. 15.

Micrograph shown in Fig. 16 represents microstructure size variation of grade 4 titanium during the rolling process. After 4 passes of rolling process the mean grain size decreased from 15 to 0.7 μm the factor of 21. Interestingly, the mean grain size of grade 4 titanium is similar with grade 2 after 4 times of rolling. It demonstrates that whether strong or soft material may have one saturation point on grain refinement in the pure titanium materials by three roll rolling process due to limited power of the roller and restricted reduction ratio of the materials. There might two

possibilities that could explain the ‘saturation’ phenomenon. Firstly, relatively high processing temperature is the one consideration that can increase the grain growth during the rolling process and caused to hinder grain refinement. Due to the rolling process only depends on a friction between rollers and materials, there are lots heat would occur during the rolling and transfer to the processing material. As a consequence some part of the material may increase temperature, especially contact surfaces area in some studies even reached to recrystallize temperature at higher temperature of rolling process[10, 11]. This kind effect is more efficient when rolling material approach to final product that causes increased temperature in whole sample. The second concernment is high strain energy during the deformation. High strain energy may save in the processing material because during the plastic deformation some of the energy will transfer to heat energy as explained above and some of rest strain energy will remain in the grain boundaries after plastic deformation which leads to a grain recrystallization process as known dynamic recrystallization (DRX)[12-14]. In this approach, low temperature process is highly recommended to get extreme fine grains with further treatment.

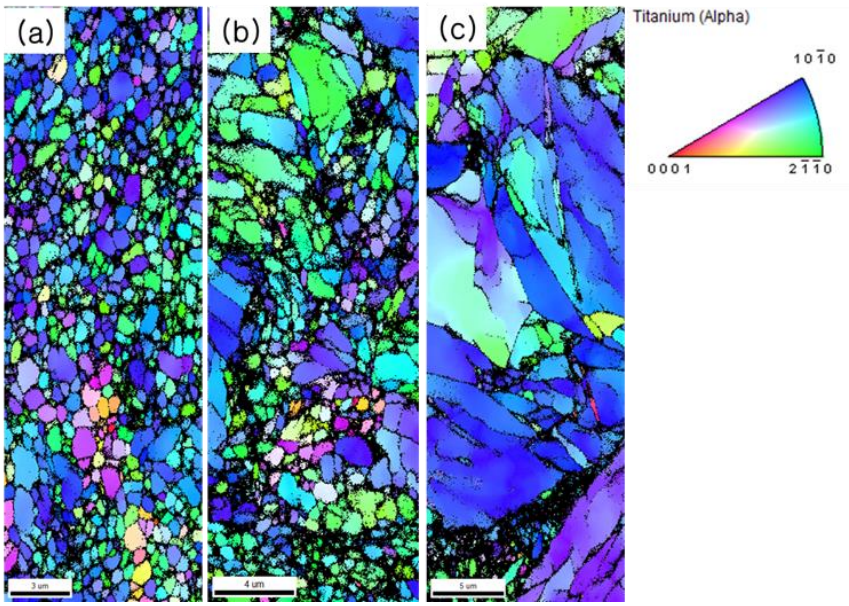


Fig. 7. EBSD micrograph of 64% reduced grade 2 titanium in rim (a), middle (b) and central (c) location at processing temperature of 350°C by 4 times of rolling.

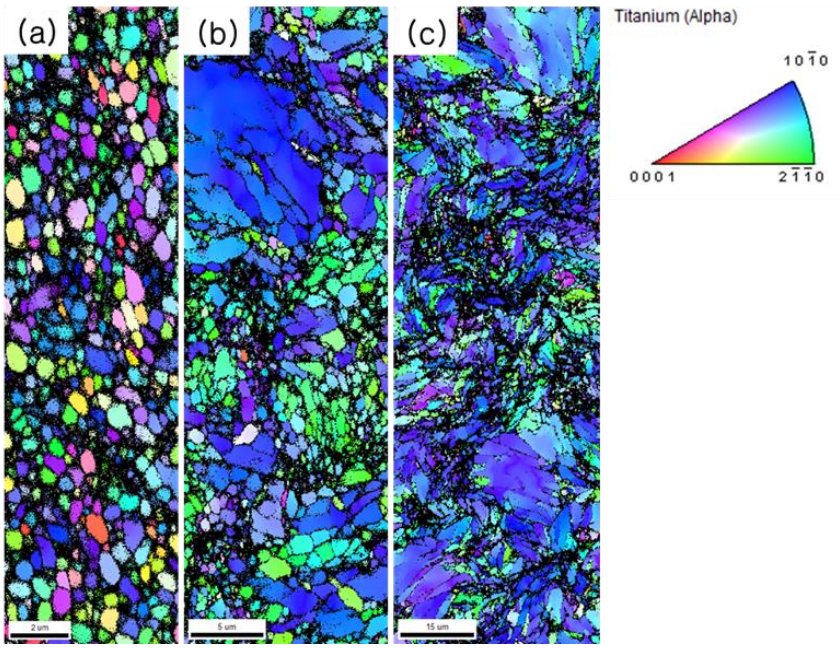


Fig. 8. EBSD micrograph of 64% reduced grade 2 titanium in rim (a), middle (b) and central (c) location at processing temperature of 400°C by 4 times of rolling.

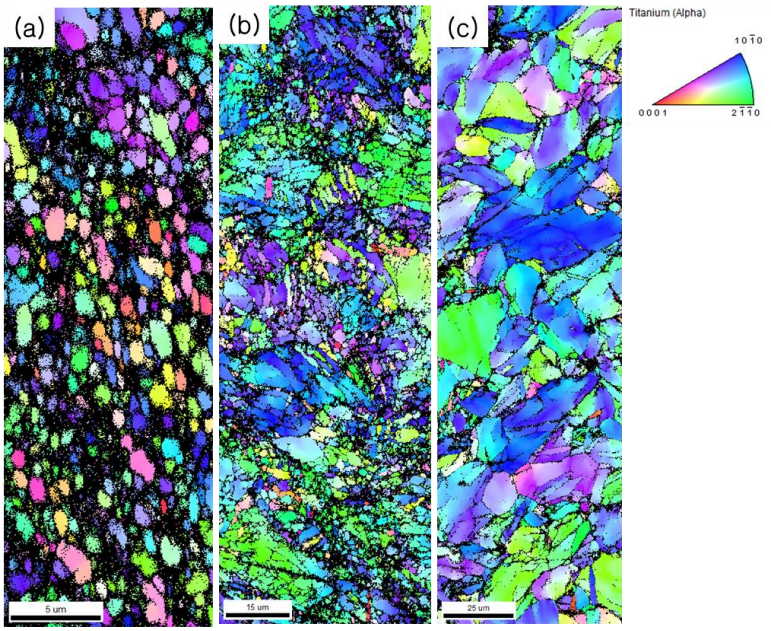


Fig. 9. EBSD micrograph of only 1 time rolled grade 2 CP Ti (from 25 mm to 22 mm of diameter) of microstructure distribution where rim (a), middle (b) and center (c) of the sample at temperature of 450 °C.

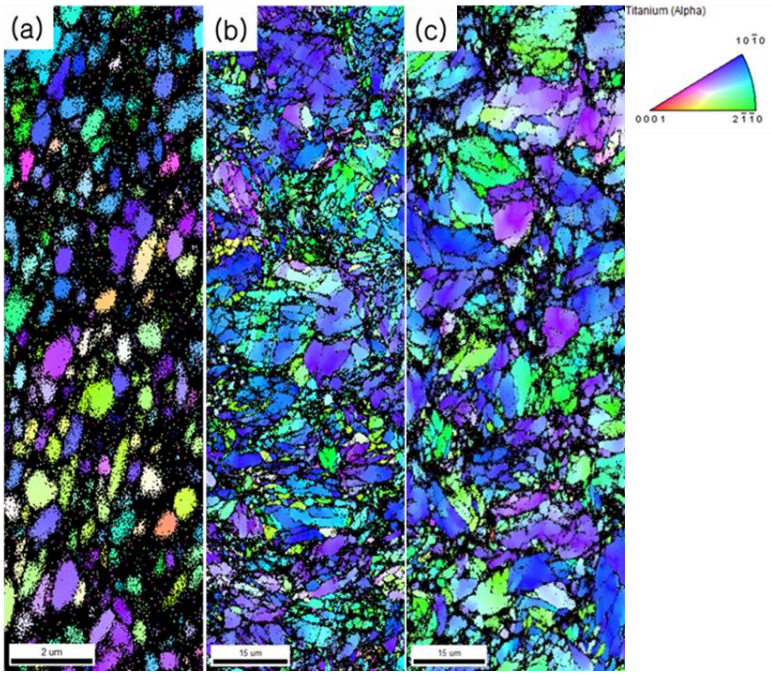


Fig. 10. EBSD micrograph of after 2 times rolled grade 2 CP Ti (from 22 mm to 20 mm of diameter) of microstructure distribution where rim (a), middle (b) and center (c) of the sample at temperature of 450 ℃.

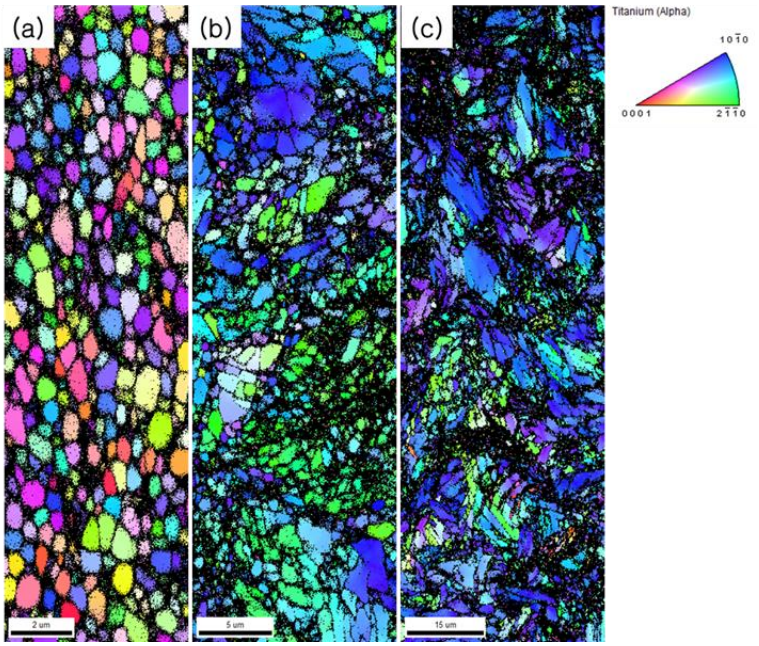


Fig. 11. EBSD micrograph of after 4 times rolled grade 2 CP Ti (from 17 mm to 15 mm of diameter) of microstructure distribution where rim (a), middle (b) and center (c) of the sample at temperature of 450 ℃.

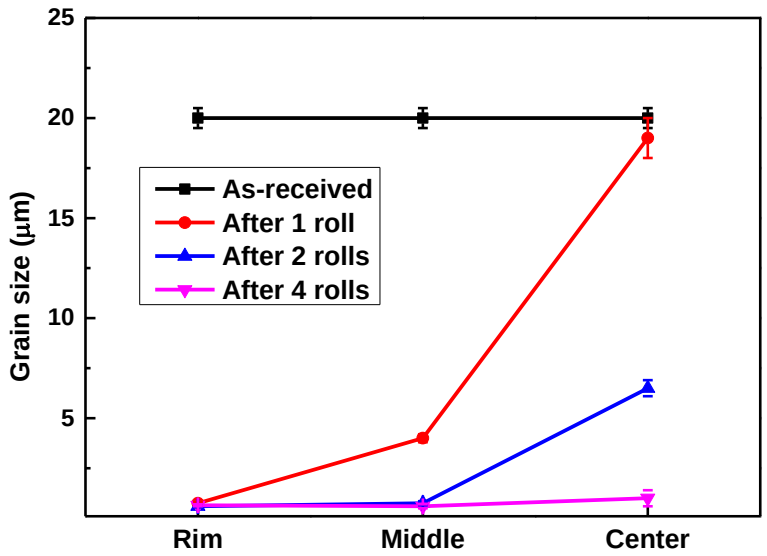


Fig. 12. Diagram of grain size variation after 1, 2, and 4 rolled grade 2 CP Ti specimen depending on different location.

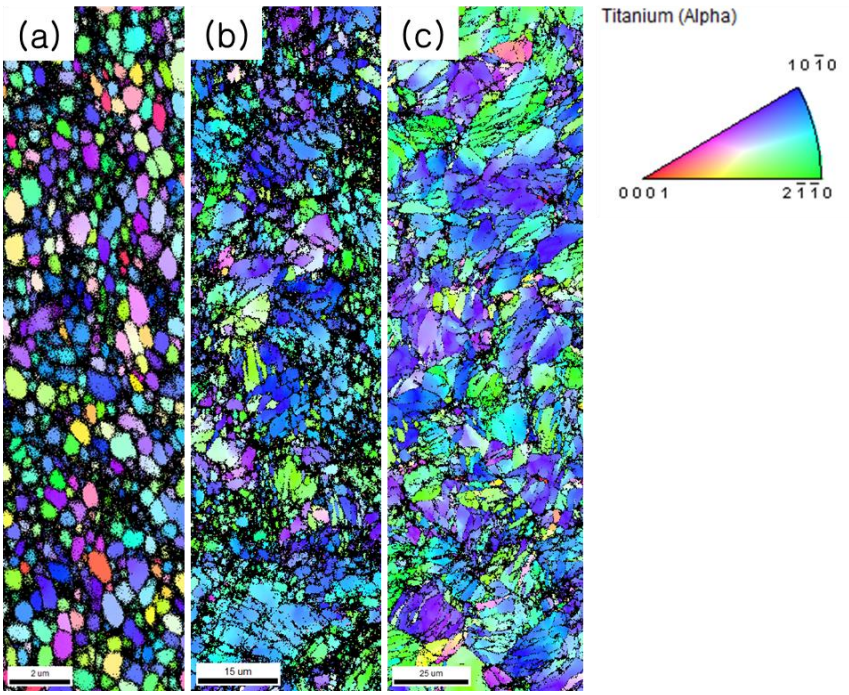


Fig. 13. EBSD micrograph of only 1 time rolled grade 4 CP Ti (from 25 mm to 22 mm of diameter) of microstructure distribution where rim (a), middle (b) and center (c) of the sample at temperature of 450 °C.

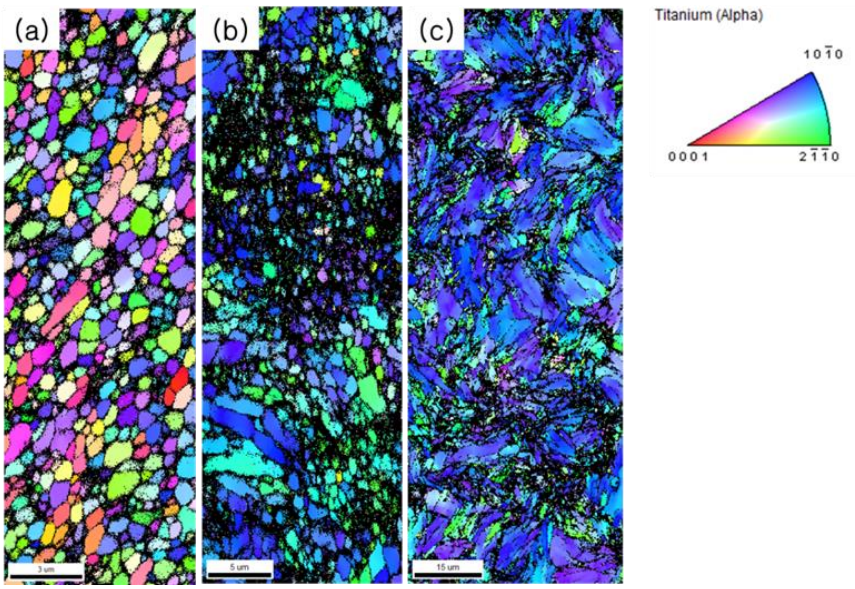


Fig. 14. EBSD micrograph of 2 times rolled grade 4 CP Ti (from 25 mm to 22 mm of diameter) of microstructure distribution where rim (a), middle (b) and center (c) of the sample at temperature of 450 ℃.

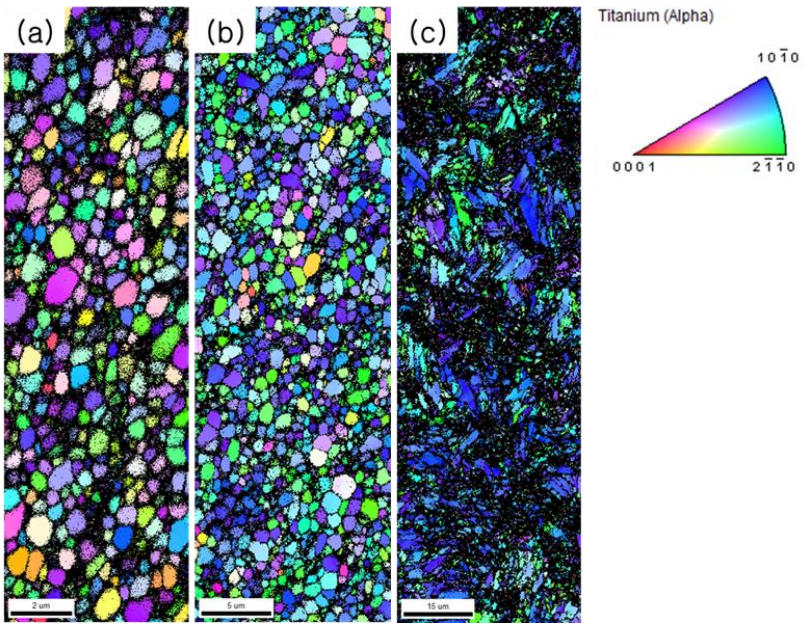


Fig. 15. EBSD micrograph of 4 times rolled grade 4 CP Ti (from 25 mm to 22 mm of diameter) of microstructure distribution where rim (a), middle (b) and center (c) of the sample at temperature of 450 ℃.

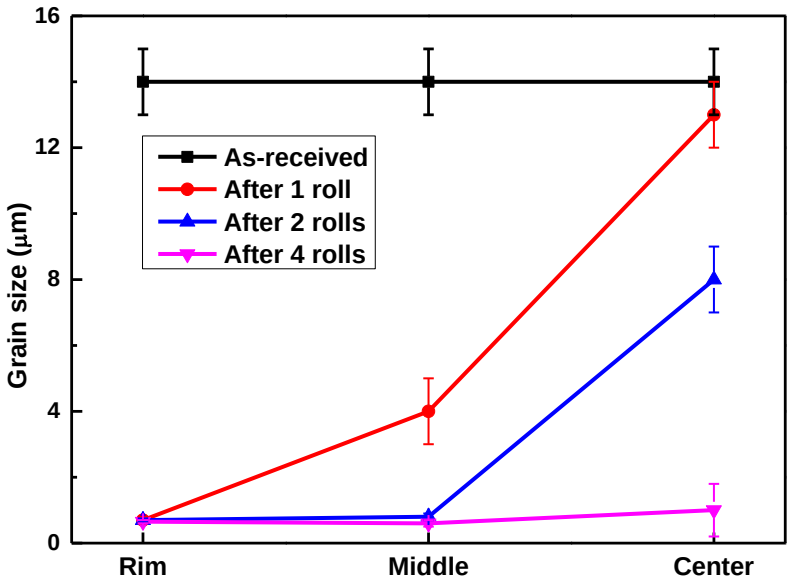


Fig. 16. Diagram of grain size variation after 1, 2, and 4 rolled grade 4 CP Ti specimen depending on different location.

### 2.3.2 Mechanical properties

Vickers hardness of the grade 2 titanium is shown in Fig.17. The Vickers hardness was increased as number of pressing increasing. In the first processing the hardness improvement was not in evidence except rim part, however after 4 times of rolling the hardness of the entire sample was increased about 45%. Depending on those results the tensile test results is shown in Fig.18. The as received grade 2 titanium has a 380 MPa and 36% of Ultimate Tensile Strength (UTS) and elongation. After 1 time rolling only rim and middle part of the area increased its strength significantly. This result accorded with microstructure observation in section 2.3.1. In further rolling, especially after 2 times rolling the ultimate tensile strength in rim, middle and center part of the sample increased to 700 MPa of strength with average value of elongation of 27%. In high concentration of strain energy may cause grain refinement and twinning effect, as a consequence coarse grains split to the new grains then new grains formed new grain boundaries that impeded dislocation movement[15]. While 4 times milled strength of the sample showed different tendency compare to 1 and 2 times milled conditions, middle part (purple line in Figure 18) showed highest ultimate strength. High temperature of the rim part during the rolling

process would give the answer on this unexpected result. In the previous literatures [10, 11] have found that temperature between three rolls and material reached to over 600 ~ 700$^{o}$C which is enough to cause not only grain growth and recrystallization but also dynamic recovery by using computer simulation and real experiment[16, 17].

Fig.19 shows Vickers hardness results of grade 4 titanium. Comparing to grade 2 titanium in hardness improvement was not so evident except rim part due to of high strength of itself. However, after 4 times rolling entire part of the material as same as grade 2 titanium has shown improvement on hardness. Tensile strength that is shown in Fig.20 also followed same trend of hardness. The more passing, the more increment of strength. This also matches with microstructure observation in above section.

Table 2 and 3 listed grain size and mechanical properties of grade 2 and 4 titanium after PSW processing. Grade 2 titanium showed superiorly improved mechanical properties especially in yield strength compare to as received condition. The yield strength increased over 100% of as received condition. While elongation was decreased about 13%, however it is acceptable as compared with losing 13% of elongation. Grade 4 titanium also showed enhanced mechanical properties in yield strength about 36% by losing 5% of

elongation. It is also acceptable because grade 4 titanium itself showed already hard to deform properties, although it only has less than 50% of increment.

Fig.21 presented ultimate tensile strength change during the 1, 2 and 4 passing of three-roll planetary rolling process. As expected, tensile strength improved with increasing number of passing. In the first trial, both grade 2 and 4 showed not much improvement on strength, however after second trail grade 2 titanium showed significantly improvement, while grade 4 titanium showed smooth improvement to the last due to its relatively large amount of impurities that impede movement of dislocations compare to grade 2 titanium.

Fig.22 illustrates the grain size variation during the PSW process. It can be found that, the average grain size reduced when increasing the times of rolling if only count the middle part of the specimens. In addition, the rim and center can be ignored due to the inhomogeneous strain distribution in the process and the major deformation part is located in the middle area. The reduction of grain size corresponds to the increment of mechanical strength as shown in Fig.21.

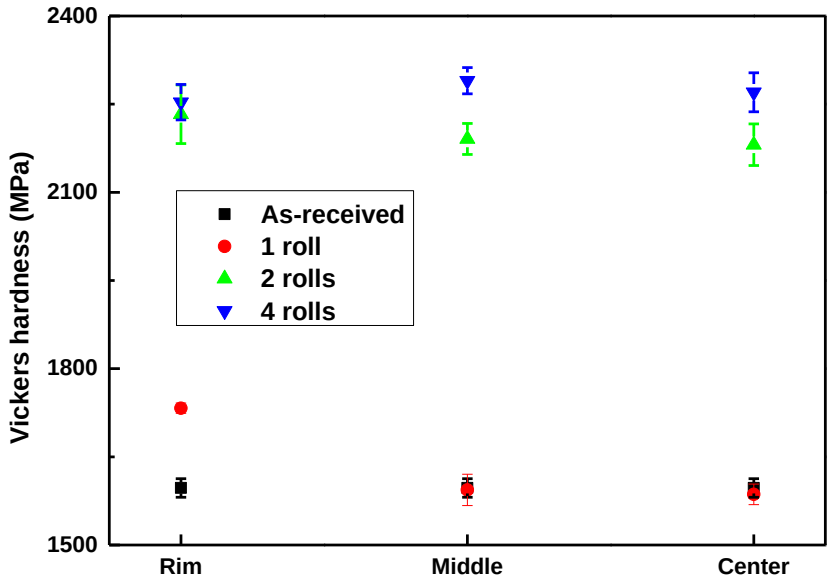


Fig. 17. Diagram of Vickers hardness variation after 1, 2 and 4 times of rolling process on grade 2 CP Ti with different locations of the specimen.

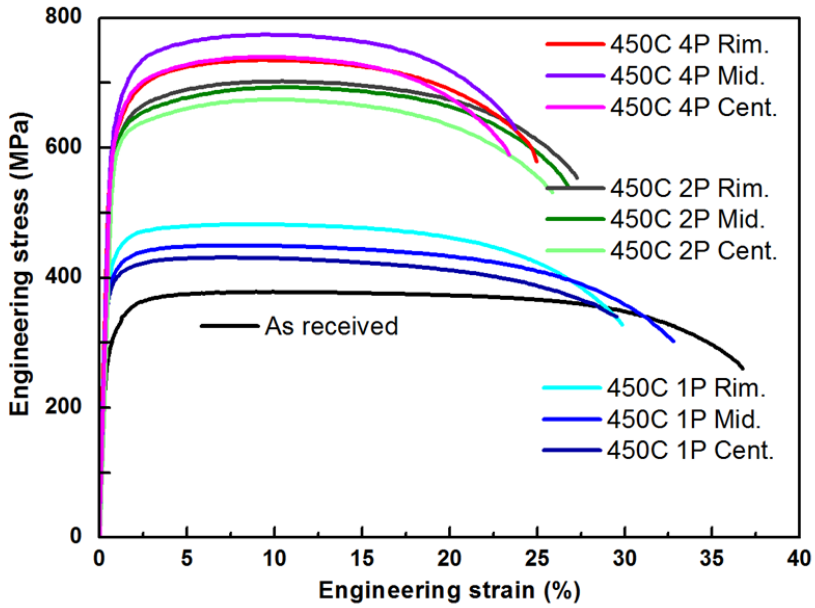


Fig. 18. Diagram of engineering stress strain curves of grade 2 CP Ti by tensile tests depending on different location of the sample after 1, 2 and 4 times processed sates.

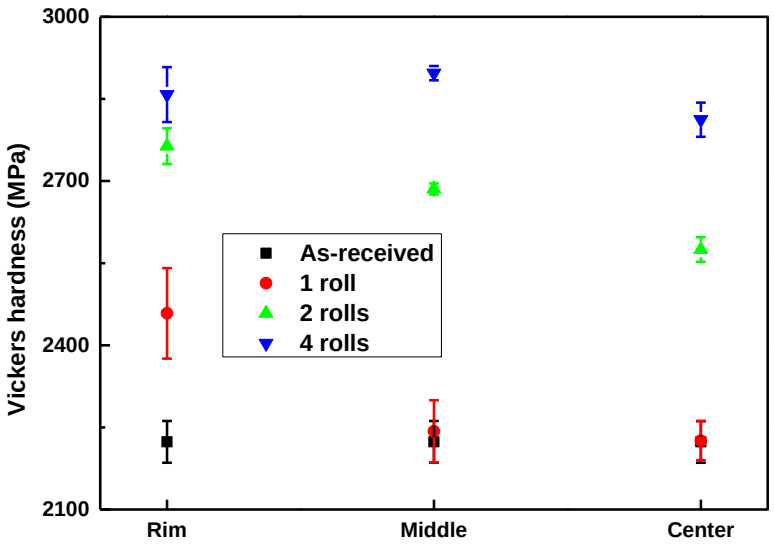


Fig. 19. Diagram of Vickers hardness variation after 1, 2 and 4 times of rolling process on grade 4 CP Ti with different locations of the specimen.

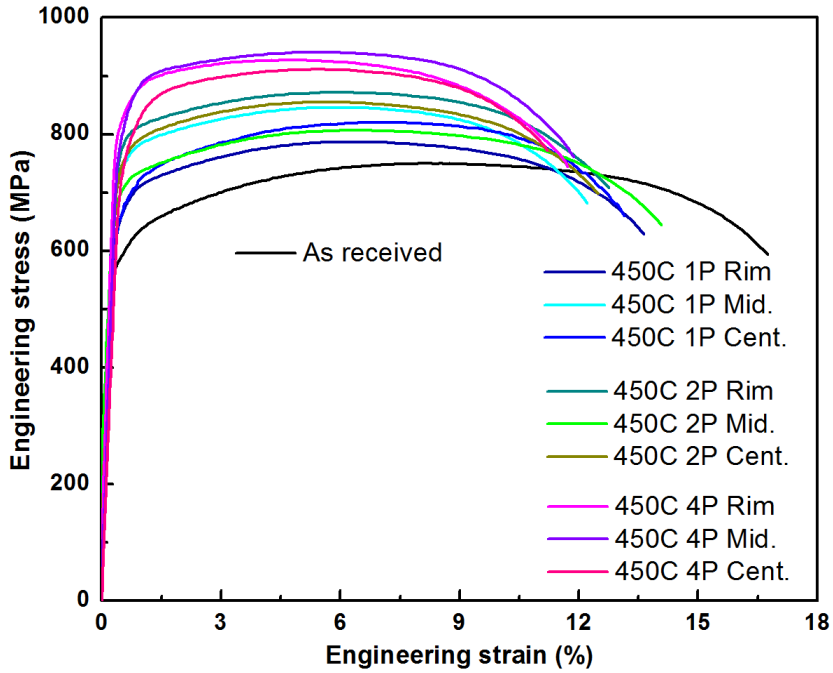


Fig. 20. Diagram of engineering stress strain curves of grade 4 CP Ti by tensile tests depending on different location of the sample after 1, 2 and 4 times processed sates.

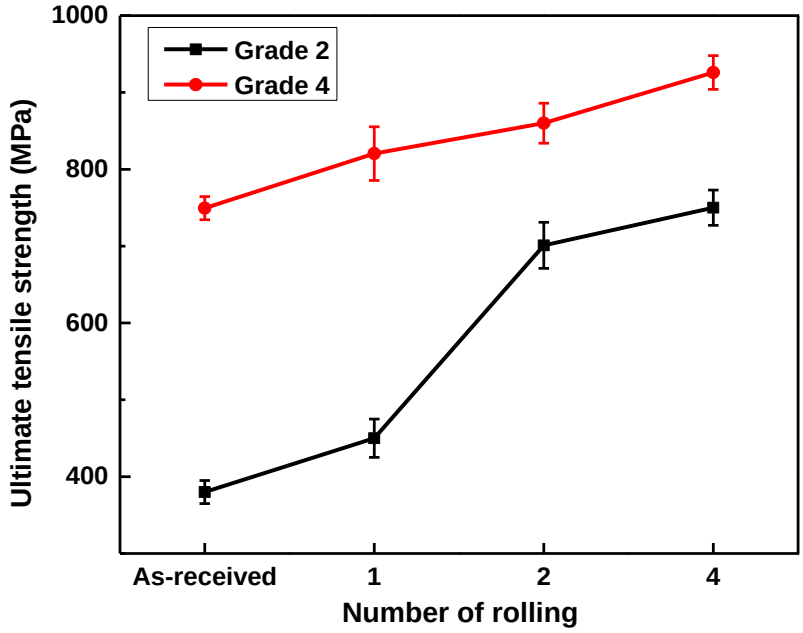


8

Fig. 21. Diagram of UTS results with after 1, 2 and 4 PSW processed grade 2 and grade 4 CP Ti. Both the grade 2 and 4 CP Ti increased strength remarkably.

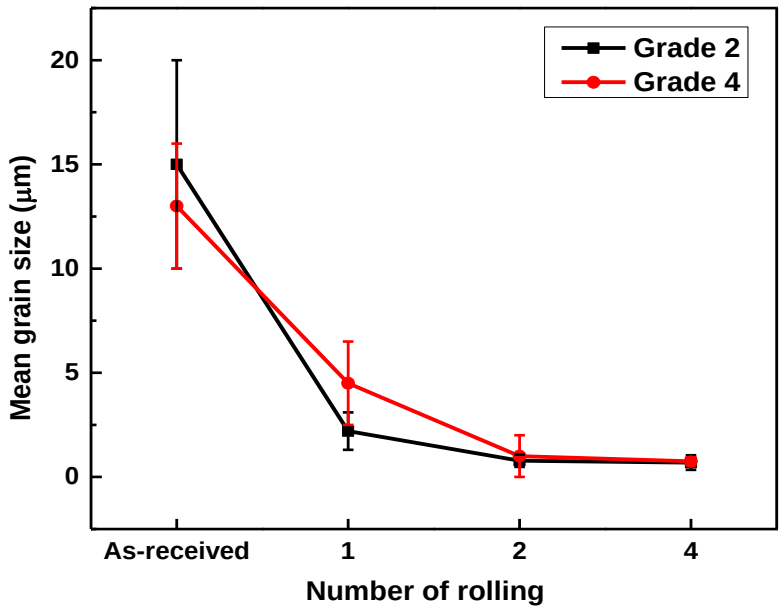


Fig. 22. Diagram of mean grain size variation after 1, 2 and 4 PSW processed grade 2 and grade 4 CP Ti where rim and central location were not involved due to the less influence of bulk materials mechanical properties depending on Fig.17, 18, 19 and 20.

Table 2. Mechanical properties of 4 PSW processed (64% reduction of cross-sectional area) of grade 2 CP Ti.

| 450 °C | Mean GS (μm) | $\sigma_{YS}$ (MPa) | $\sigma_{UTS}$ (MPa) | $\delta_{Eng}$ (%) |
|---|---|---|---|---|
| As received | 16 | 278.2 | 378 | 36.7 |
| Rim | 0.65 | 605.9 | 734.6 | 24.9 |
| Middle | 0.6 | 628.7 | 773.3 | 23.7 |
| Center | 1 | 609.6 | 739.5 | 23.4 |
| Average | 0.75 | 614.7 | 749.1 | 24 |

Table 3. Mechanical properties of 4 PSW processed (64% reduction of cross-sectional area) of grade 4 CP Ti.

| 450 °C | Mean GS (μm) | $\sigma_{YS}$ (MPa) | $\sigma_{UTS}$ (MPa) | $\delta_{Eng}$ (%) |
|---|---|---|---|---|
| As received | 14.5 | 600.7 | 749.5 | 16.8 |
| Outer | 0.6 | 839.2 | 926.8 | 11.7 |
| Middle | 0.7 | 836.6 | 940.1 | 11.9 |
| Center | 1 | 779.1 | 910.9 | 11.2 |
| Average | 0.77 | 818.3 | 925.9 | 11.6 |

## 2.4 Conclusions

Mechanical properties CP titanium grade 2 and 4 were successfully enhanced by grain refinement using three roll planetary rolling process. The mean grain size decreased from 20 to 0.75 μm and the yield strength enhanced from 278.2 to 614.7 MPa in grade 2 titanium. Grade 4 titanium also showed refined grain size from 15 to 0.77 μm and yield strength improved from 600.7 to 818.3 MPa. These results in a relatively good agreement with numerical calculation of Hall-petch relationship, notably the theoretical value ($\sigma y \approx 576$ MPa and $\sigma y \approx 646$ in grade 2 and 4 by using given value[18], respectively) are not perfectly match with experimentally measured one. None uniformity of the PSW process and texture effect may are the considerable reasons causing distinction between theoretical and experimental results. Eventually, however, all part of the materials was showed a quite homogenous microstructure distribution and strength after 64% of reduction, although it showed inhomogeneous mechanical properties in the beginning of the process.

## 3. Finite element analysis (FEA) simulations

### 3.1 Back ground of FEA simulation

FEA is the one of the most popular simulation methods. In 1960s, Clough has mentions about this method firstly. It is the idea that when we face complicated and hard calculation to separate all the boundary condition and also consider the relationship between each components in order to have the solutions by finite element method. This method already has over 30 years of historical development; however there was no good prospect in the beginning due to of limitation on computer technology. But it stood its head 1990s when computer technology developed in marvelously expeditious progress. So far, FEA method already propagated in extreme speed and applied in more and more science and technology area for prediction. Nowadays, FEA method can systemically analysis many kinds of simulation areas, for example heat flow, stress and strain calculations in 3D scale. There is lots of software that most of them based on Largrange function in commercial sale like MSC, ANSYS, ABAQUS, I-DEAS and DEFROM etc.

In this paper DEFORM-3D by SFTC was hired to investigate three roll planetary rolling process. DEFORM-3D is a finite element

method based process simulation system designed to analyze various forming and heat treatment processes used by metal forming and related industries. The simulation process would separate to 3 major steps as shown in Fig.23. The first step is called pre-processing that includes creating a geometric design by professional CAD/CAM software, inputting thermal and mechanical properties on the work pieces, meshing the targeted material, controlling simulation steps, and considering the environment and interface of objective variables. After gathering those parameters, it will found a database and begins to run simulation by selected solvers (Conjugate-Gradient or Sparse). Conjugate-Gradient method is an algorithm for the numerical solution of particular systems of linear equations[19]. The conjugate method is an interactive method, so it can be applied to sparse systems that are too large to be handled by direct methods. So, conjugate method used to calculate huge matters effectively, but it needs long times to solve. While Sparse find the accurate solution directly by using inverse matrix, however this method is more efficient on less meshed problems. The final step is named as post-processing that is used to view and extract data from the simulation results in the database file. All results steps that were saved by the simulation engine are available in the post-processor. Deformed

geometry, boundary plots, vector plots, and flow net, state variable and image data can also be extracted in a number of neutral formats for use with other programs.

In the three roll planetary rolling simulation Sparse method was hired to calculate the problem due to less elements (mesh number of 100,000). There are lots of parameters that influence the material deformation in real experimental process, however in simulation some of them are ignored or assumed artificially in order to easy calculation to save time. In this study few of parameters were assumed as below[20, 21].

1) Elasticity of the materials was ignored because of tiny change.
2) The deformation of the material follows Levy-Mises flow stress theory.
3) The material has isotropic deformation during the process.
4) The volume of the material keeps same value.
5) Ignoring the inertial and body force.

Depending on the above assumption, the processing material could consider as a rigid plastic body that can satisfy the plasticity

equation shown below[22] and solved with direct interaction method eventually.

1) The equilibrium differential equation (motion of equation)

$$\sigma_{ij,j} + f_i = 0 \qquad (3\text{-}1)$$

2) Geometry function

$$\dot{\varepsilon} = \frac{1}{2}(v_{i,j} + v_{j,i}) \qquad (3\text{-}2)$$

3) Constant volume

$$\dot{\varepsilon_{ij}}\delta_{ij} = 0 \qquad (3\text{-}3)$$

4) Constitutive equation of rigid plastic body

$$\dot{\varepsilon_{ij}} = \frac{3}{2}\frac{\dot{\bar{\varepsilon}}}{\bar{\sigma}}\grave{\sigma}_{ij} \qquad (3\text{-}4)$$

Where, $\bar{\sigma} = \sqrt{\frac{3}{2}\grave{\sigma_{ij}}\grave{\sigma_{ij}}}$ is equivalent stress, and $\bar{\sigma} = \sqrt{\frac{3}{2}\dot{\varepsilon}_{ij}\dot{\varepsilon}_{ij}}$ is equivalent strain rate

5) Mises yield criteria in rigid plastic material

$$\bar{\sigma} = \sqrt{\frac{3}{2}\grave{\sigma_{ij}}\grave{\sigma_{ij}}} = f(\bar{\sigma}) \qquad (3\text{-}5)$$

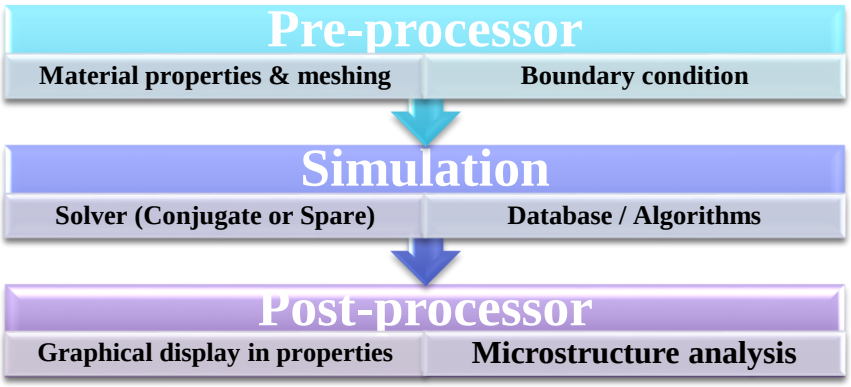


Fig. 23. Schematic diagram of FEA simulation procedure in DEFORM-3D.

### 3.2 Modeling of three roll planetary rolling

Fig.24 is the real experimental three roll planetary rolling equipment. As shown in the figure, three rollers rotate by three equally arranged axes. Creating a 3D modeling is a complicated procedure due to the coordinate transformation. And DEFROM-3D does not have the geometry foundation of models. So, in this study the model was created by one of the CAD/CAM software called ‘Solidworks’. The assembled model was exported as STL format that the shape of the each part is shown in Fig.25. The dimension of the titanium bar is 25 mm in diameter and 150 mm in length. Most of the previous researches [23-25] have set the initial head part as corn shape in order to improve the friction between rollers and work piece. Hydrostatic backpressure force (10 N) was added to escape the friction problem until the three rollers bite the work piece and pressing the sample automatically.

Fig.25 (b) shows the rotation axes of three rollers and work piece. The rotation axes of rollers were calculated by homogeneous transformation matrix with offset and inclined angle. Fig.26 represents the 3D coordinate transformation using (X, Y, Z) axes. The transformed new axes would be written as below.

$$(X'\ Y'\ Z'1) = (X\ Y\ Z\ 1) \cdot Rx(X,\alpha) \cdot Ry(Y,\beta) \cdot Rz(Z,\gamma) \cdot T(a,b,c)$$

Where Rx is rotation of X-axis by angle α

$$Rx(X,\alpha) = \begin{bmatrix} 1 & 0 & 0 & 0 \\ 0 & cos\alpha & sin\alpha & 0 \\ 0 & -sin\alpha & cos\alpha & 0 \\ 0 & 0 & 0 & 1 \end{bmatrix}$$

Ry is rotation of Y-axis by angle β

$$Ry(Y,\beta) = \begin{bmatrix} cos\beta & 0 & -sin\beta & 0 \\ 0 & 1 & 0 & 0 \\ sin\beta & 0 & cos\beta & 0 \\ 0 & 0 & 0 & 1 \end{bmatrix}$$

Rz is rotation of Z-axis by angle γ

$$Rz(Z,\gamma) = \begin{bmatrix} cos\gamma & sin\gamma & 0 & 0 \\ -sin\gamma & cos\gamma & 0 & 0 \\ 0 & 0 & 1 & 0 \\ 0 & 0 & 0 & 1 \end{bmatrix}$$

T (a, b, c) is the transformation to the original point.

$$T(a,b,c) = \begin{bmatrix} 1 & 0 & 0 & 0 \\ 0 & 1 & 0 & 0 \\ 0 & 0 & 1 & 0 \\ a & b & c & 1 \end{bmatrix}$$

The rotation axes of the three rollers were calculated by ‘Mathmatica’ software in this modeling.

200,000 triangular meshes had applied to work piece and three rollers were set as rigid body. The rotation speed of each roller was set to 120 RPM clockwise as shown in Fig.25 (c). The coefficient of friction between rollers and work piece is major factor that highly influence the simulation results because slip will occur during the process if the friction is to low and causing failure. In previous simulations[1, 26], it has been recommended the value of coefficient of friction as 0.9 because of under 5% of speed error between work piece and rollers. The offset angle α and inclined β angle were set to 9.5° and 16.5°. The mechanical properties of the work piece were collected from DEFROM-3D material database named as 'Ti type Π (200 – 1100°C)' which corresponding grade 2 titanium and grade 4 titanium was not involved in this study because of same expectation of simulation results depending on the real experiment. The work piece had 450°C of initial temperature and heat transfer coefficient and convective heat transfer coefficient for every part set to 5 W/m°C and 0.02624 W/m°C, respectively, then simulation was conducted at atmosphere (20°C) condition. Whole simulation had about 100 steps and each step has 0.01s of continuous increment.

The microstructure modeling features of the DEFORM-3D Post-Processor including prediction of work hardening, grain boundary

misorientations, grain shapes, recovery, recrystallization, and more (such as precipitation, phase transformation).

There are various established algorithms to simulate reactions between lattices during the plastic deformation. Most well-known three of these are Cellular Automata (CA), the Monte Carlo, and the Phase Field algorithms. At present, CA is the only implemented algorithm. CA involves calculating the state of a local cell as a function of external inputs (such as strain, strain rate, and temperature) and the states of its local neighbors. If a particular cell switches state (for example, recrystallizes, or changes phase), then its neighbors will follow as well. It is a computationally efficient algorithm which provides a reasonable level of detail. Since reactions permeate through a CA via calculations with its neighbors, the shape of the reaction front will be a function of the number of neighbors, number of nearest neighbors, and their connectivity. In this model, a square lattice which only computes its local state as a function of its nearest neighbors (each cell only have four neighbors) was considered as discrete lattice geometry. In this consideration, Moore's Neighborhood (see Fig.27) chose for discrete lattice neighborhood and Periodic, warp-around boundary condition was selected to

simulate propagation of transforming fronts (recrystallization fronts, phase transformation fronts, etc) at the boundaries.

Depending on above instructions, three different point were tracked in order to observe microstructure variation as shown in Fig.28 and radius of the Moore's Neighbor was defined as default value of 1 and, then, the resolution of the discrete lattice was settled by 150×150 μm of a region of material in this microstructure simulation.

Dislocation density constants are the main factor which highly influences the simulation results because the mechanism for accommodation of actual deformation at the microstructure level in a material is the movement, generation and annihilation of dislocations. Dislocations are "Kinks" in the atomic structure which permit atom planes in a crystal to slip past each other under pressure. During the deformation and heat treatment of a material, dislocation may generate and annihilate due to hardening and recovery effects. The resultant sum, among other things, determines the hardening behavior of the material. Additionally, dislocation density can be a measure of the threshold for nucleation of recrystallization. There are two common "hardening and recovery" models for dislocation density calculation which are the Laasraoui-Jonas and Kocks-Mecking model.

At present study, discrete lattice microstructure model was modified by Laasraoui-Jonas model, detailed below.

The dislocation density for each region of a microstructure is calculated as a function of hardening and recovery with respect to strain (equation 1). The hardening and recovery terms themselves are functions of strain rate and temperature (equation 2 and 3).

$$d\rho_i = (h - r\rho_i)d\varepsilon \qquad (1)$$

$$h = h_0 \left(\frac{\dot{\varepsilon}}{\dot{\varepsilon}_0}\right)^m exp\left(\frac{mQ}{RT}\right) \qquad (2)$$

$$r = r_0 \left(\frac{\dot{\varepsilon}}{\dot{\varepsilon}_0}\right)^{-m} exp\left(\frac{-mQ}{RT}\right) \qquad (3)$$

Where *m, Q, $h_0$, $r_0$* and $\dot{\varepsilon}_0$ are hardening sensitivity, activation energy, hardening constant, recovery constant and strain rate calibration constant respectively. The detailed values of these constants were presented in Table 4 which some of them were obtained from references and the others were gained from user-input of experimental data by inverse analysis method. Additionally, the initial value for dislocation density ($\rho_i$) must be specified. In this model typically value of the annealed metal was taken as 0.01 $\mu m^2/\mu m^3$. The discrete lattice CA microstructure model employs a modified version of the Laasraoui-Jonas hardening and recovery

model, where by the cells in which recovery occur are randomly. This results in a non-uniform dislocation distribution conducive to initiating recrystallization. This algorithm involves the selection of a certain number of cells $N_r$ during each time step, where $N_r$ is given by following equation 4.

$$N_r = \left[\frac{(\#Rows)\times(\#Columns)\times\sqrt{2}}{K}\right]^2 h(d\varepsilon)^{(1-2m)} \qquad (4)$$

Where $K$ is user-specified [ref 'modeling dynamic recrystallization using cellular automata].

During the deformation and heat-treatment, recrystallization of various sorts may occur for example, Discontinuous Dynamic Recrystallization (DDRX), Continuous Dynamic Recrystallization (CDRX), Geometric Dynamic Recrystallization (GDRX), and Static Recrystallization (SRX)[27-31]. In the simulation and real experimental process SRX were ignored due to the processing temperature which is much lower than elevated temperature. Unfortunately, at present simulation only DDRX was chose for microstructure simulation because the DEFORM-3D program have not implement other recrystallization option yet. Therefore, this program is not so reliable with lower temperature plastic deformation simulation. In this consideration, the microstructure evolution

simulation in this study is not perfectly match with actual experiments, however, we can obtain the trend and distribution of none uniformly deformed grains that are one of the main purposes of this simulation due to the different flow stress and strain during the deformation.

As described above, the dislocation density calculation determines the stored energy in the material which depending on the recrystallization phenomena selected above, different types of recrystallization can occur and as mentioned before DDRX model was chose in this study with a function of threshold dislocation density and probability, whereby only a statistical fraction of the local regions which reach a critical dislocation density threshold become recrystallizing nuclei. For this model, the critical dislocation densities necessary to nucleate recrystallized grains and probability of nucleation value were set to 0.02 and 0.01 which means that for every 100 possible nucleation sites, only one will actually nucleate a new grain). Classically, grain boundary migration (grain growth) is a function of local grain boundary curvature, as well, but at present this option was not implemented yet. Thus, in this model, the constant (default) value of 1 selected in migration velocity of grain boundaries for convenient.

Once the microstructure has evolved due to the phenomena selected above, the materials constants necessary for calculating the flow stress must be define as a function of microstructure evolution. For this model, the flow stress was defined as following; at lower temperature (below 200°C) 450 MPa; at higher temperature (above 400°C) 220MPa depending on the referee[32]. In addition, the remaining constants and proper properties for the material were defined from real experimental and characteristic of the material which also represented in Table 4.

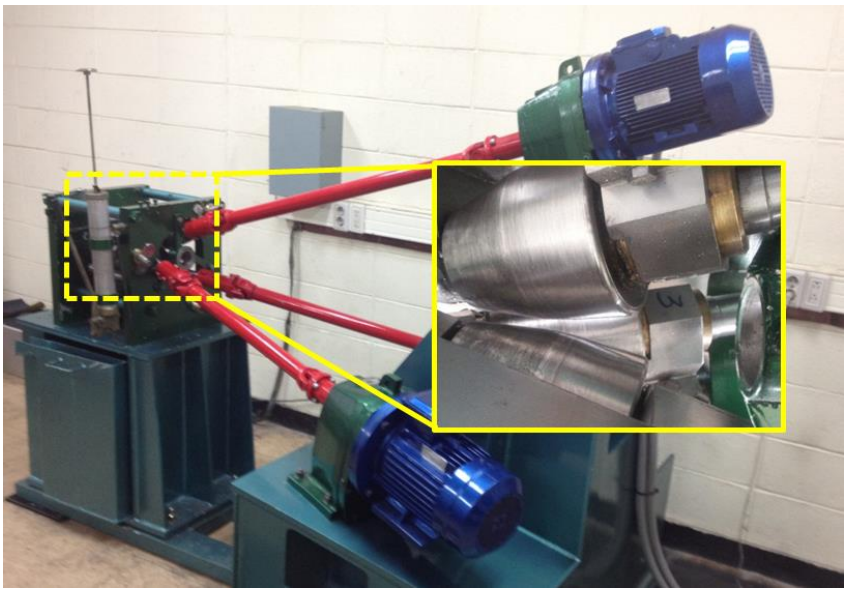

Fig. 24. The photograph of real equipment of PSW process with detailed placemnt of three rollers in side view.

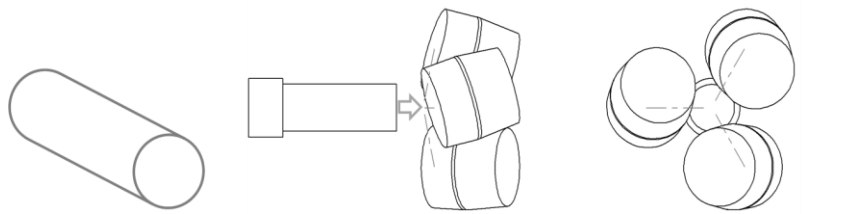


Fig. 25. A 3D-Sketches of modeling of PSW process using ‘Solidworks’ CAD software where work piece (titanium rod) (a), side view of the process (b) and front view of process.

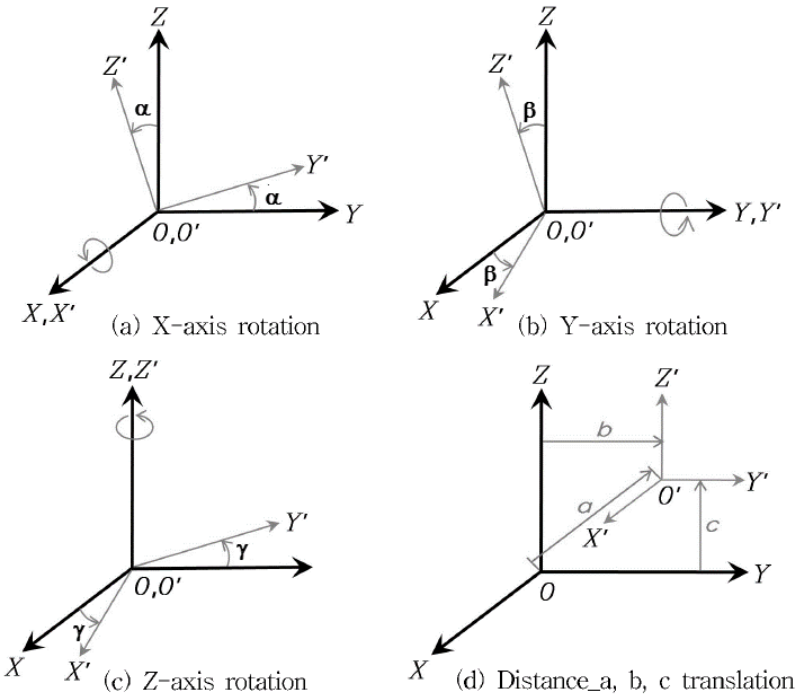


Fig. 26. Schematic diagram of transformation coordinate systems depending on different axes.

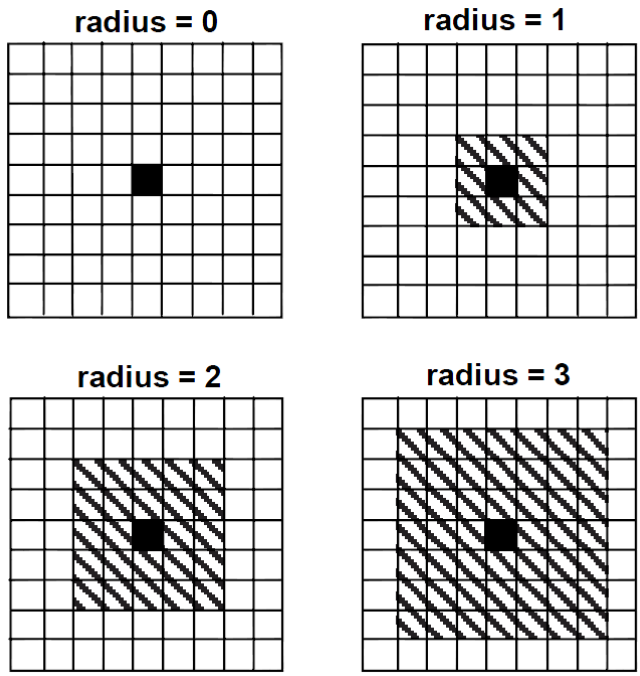


Fig. 27. A diagram of Moore's Neighborhood grain boundaries algorithm.

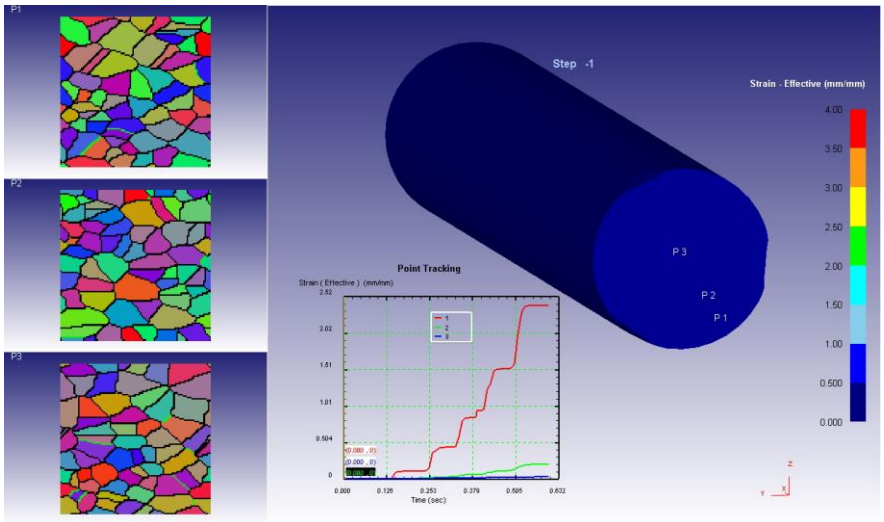


Fig. 28. Point tracking of the initial work piece P1 (rim), P2 (middle) and P3 (center) location in order to observe the microstructure evolution during the process where initial grain size are same and texture effect did not included.

### 3.3 Analysis of modeling results and discussions

Fig.29 presents cross-sectional effective stress distribution which is perpendicular to the rolling direction during the deformation in computer simulation. Four steps were captured from the simulation process as shown in figure beginning (a), one-third (b), two-third (c), and one round (d) rotation of the work piece in order to observe the stress variation. As expectation, the highest effective stresses only appeared in the interface between rollers and work piece in the beginning of deformation. After one-third of rotation of work piece effective stress slowly evolved to the sample with a triangle distribution. After two-third of rotation, the effective stress much more developed to the wide area of the sample and the triangle stress distribution area which has lower stress around center become much smaller compare to one-third rotation at the same time, while the maximum effective stress spread from contact interfaces. Finally, after one round rotation of sample, the maximum effective stress occurred in middle area of whole work pieces. Interestingly, center of the sample had almost none stress (or very low) which means that whether apply external force to the sample, the center still maintain lowest stress. However, it can be expected that center may also receive higher stress with repeating the rolling process by reducing

cross-sectional area although the effect will be less efficient compare to other area. A noticeable result from the effective stress simulation is that during the process the highest stress occurred between the rim and center area not the surface area (interface between rollers and work pieces).

Effective strain also presented in Fig.30 with same step of effective stress in order to observe the strain deviation and compare the distribution of stress and strain. In contrast, highest effective strain only showed in surface area especially interface between rollers and sample. Furthermore, the center almost maintained same strain value (close to zero) which seems to be staying on a hydrostatic condition and even rim area did not reached much of strain to the middle area after one round of rotation (d). In other words, the distribution of plastic strain along the work piece radius after the rolling is fall down with decrease of the radius and highest value of accumulated plastic strain localized only near the surface of the sample. Therefore, it was obvious from what the microstructure observation in figures above that the rim area should show the smallest grains due to the high strain in the beginning and middle area has the gradual change in the grain size with repeating the process by high stress exactly matches with microstructure evolution.

Temperature is another important parameter that could highly effect the deformation results and it is hardly to observe in the real experiments because lot amount of heat will generate during the process by friction of rollers and work piece. So temperature distribution also observed from the computer calculation for confirming the less influence of the temperature effect during the process. Fig.31 (a), (b), (c) and (d) shows the same step above of initial, one-third, two-third and one round rogation respectively. As from these figures temperature slowly increased with rotation of the work piece, however, the highest temperature always showed only at contact interface. While, after one round rotation, the rim part seems to have over 100°C of temperature compare to original temperature of 450°C in Fig.31 (d). The temperature distribution still maintained same distribution up to last reduction which will showing by following figure. In this consideration, the temperature parameter could be neglectful in the real experiment and computer simulation because the highest temperature is lower than SRX temperature.

Fig.32 shows the step which is once the work piece almost reduce its radius to final dimension that corresponds to first reduction (22% of reduction ratio) in chapter 2.2 above. Effective stress (a) indicate that the middle area has the maximum deformation effect

because highest value of effective stress occurred in the middle area on the sample, while rim area has lower stress than middle area then center has the lowest stress. As expectation, maximum plastic strain still kept in the surface of the work piece which is showing in (b) and these strain energy transfers to heat energy as a consequences the surface of the work piece increases temperature. However, temperature of the work piece (as shown in (c)) after the reduction still maintain less than 600°C except contact interface which did not reached to SRX temperature. So, it is acceptable to ignore temperature effect during the three roll planetary rolling process in this study. The heterogeneous microstructure (Fig.32 (d) P1, P2, and P3) was obtained in the microstructure simulation even though it was on the insufficient condition by applying only the DRX. At surface point P1 and P2 grain refinement occurred by the high strain and stress while center P3 combined with coarse and small grains together. Even so, the center of the material also increased the strength in the real experimental measurement in above results because in the real plastic deformation the mechanisms of strengthening involves work hardening, twinning hardening (at low temperature deformation), and texture hardening[17, 33] except grain boundary strengthening and usually strengthened material includes

combination of these strengthening mechanisms. In this sense, microstructure evolutional simulation is always the difficult and main issue due to the complicated parameters.

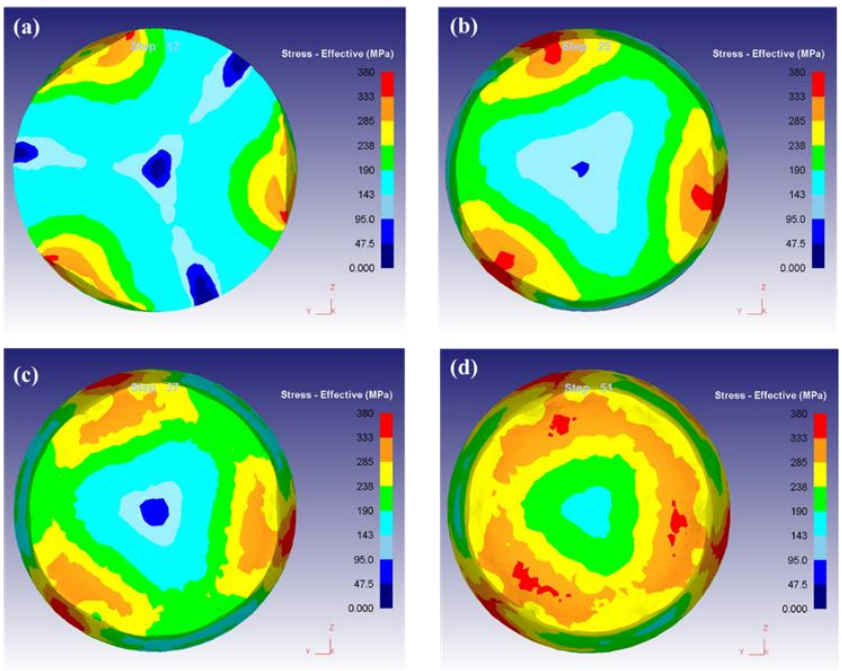


Fig. 29. Effective stress distribution of initial (a), one-third (b), two-third (c), and one round rotation (d) of work piece during the process.

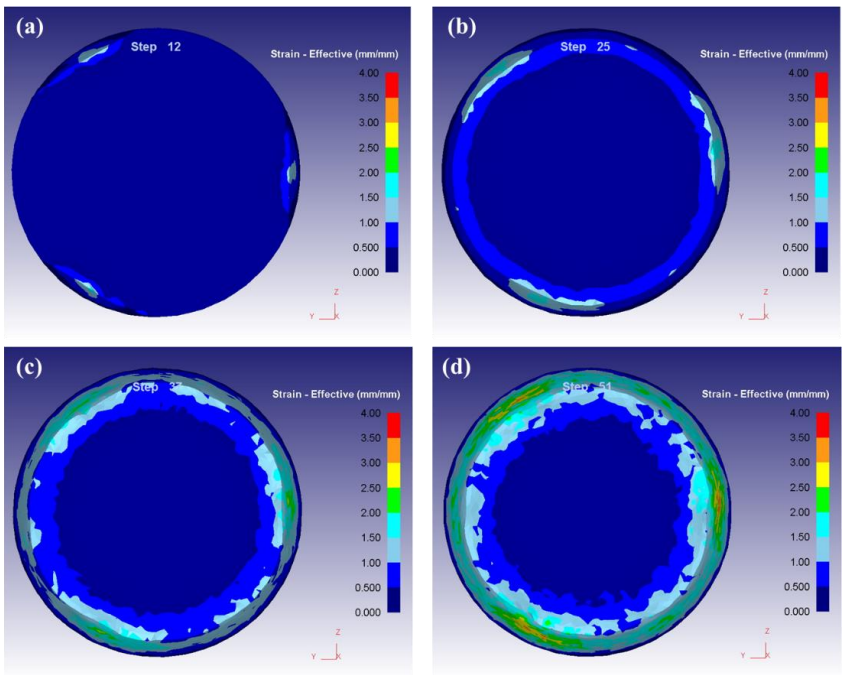


Fig. 30. Effective strain distribution of initial (a), one-third (b), two-third (c), and one round rotation (d) of work piece during the process.

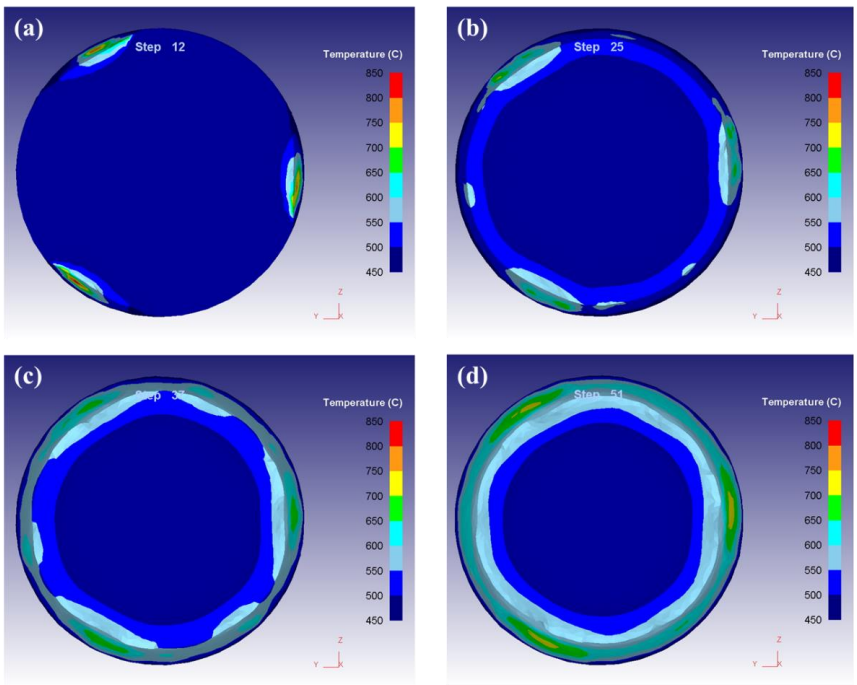


Fig.31. Temperature variation of initial (a), one-third (b), two-third (c), and one round rotation (d) of work piece during the process.

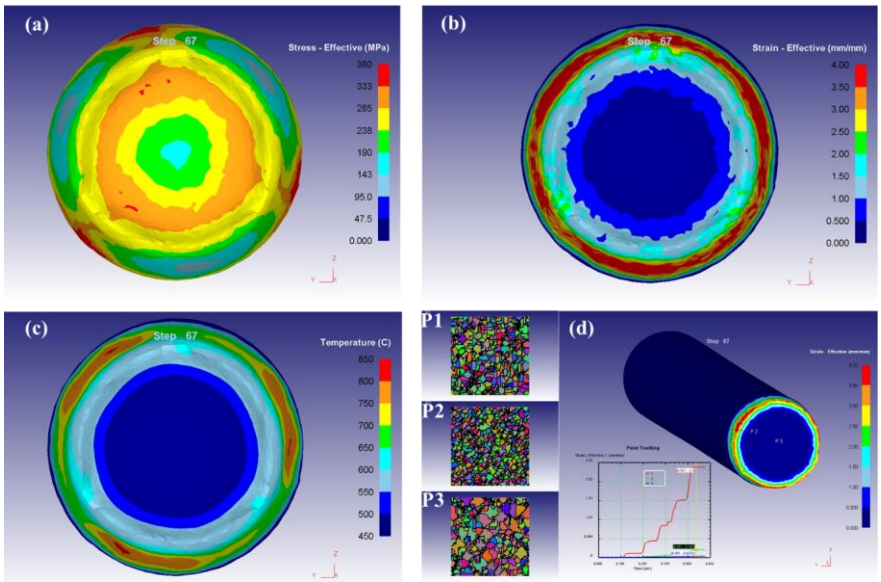


Fig.32. Diagram of effective stress (a), effective strain (b), temperature distribution (c) and microstructure evolution (d) one the work piece reach to final diameter of reduction.

### 3.4 Conclusions

The deformation behavior of CP-Ti was observed by computer calculation depending on stress-strain-temperature and microstructure evolution was monitored by CA model. The three roll planetary rolling process had an inhomogeneous plastic stress and strain during the simulation which corresponds to the heterogeneous microstructure formation at the beginning of the real experiment in above section while the temperature is a negligible parameter in spite of concerning. The microstructure evolutionary simulation result was similar with actual experimental condition; however, due to the program limitation it is still insufficient to explain the real condition.

# Chapter Ⅱ.

# Enhancement of mechanical properties of titanium by equal channel angular pressing using encapsulation method

# 1. Introduction

## 1.1 Background of equal channel angular pressing

UFG materials can be defined as polycrystalline materials which are composed with very fine grains and have huge amount of grain boundary area. The grain size is in the submicron rage even can go down to nanometer scale as well. Usually, nano crystalline materials contain grains with in average grain size less than few hundred nanometers. The presence of fine grains and large grain boundary area results in improved physical and mechanical properties [34-43]. Several fabrication techniques are currently available to produce nano structured material and these processes can be generally classified into the following five groups as mechanical milling and compaction, severe plastic deformation, consolidation via severe plastic deformation, inert gas condensation of particulates and consolidation and electro deposition. Whereas the first two methods typically tend to increase yield material with UFG structure, the latter three techniques are capable of producing material with and average grain size of ten nanometers. Each of these methods has advantages and disadvantages and one should choose the appropriate method depending upon the material design attributes. In order to convert a

coarse-grained solid into a materials with UFG structure, it is necessary both to impose and exceptionally high strain for introducing a high density of dislocations and for these dislocations to subsequently rearrange to form and array of new grain boundaries. In practical, however, conventional metal working procedures, such as extrusion or rolling, are restricted in their ability to produce UFG materials in two important reasons. The first limitation is that there is a limitation on the overall strains that may be imposed using these procedures due to the processing techniques incorporate corresponding reductions in the cross-sectional dimensions of the work pieces. Secondly, the strains imposed in conventional processing are insufficient to introduce UFG structures since the generally low workability of hard-to-deform materials at ambient and relatively low temperatures. As a consequence of these limitations, attention has been devoted instead of the development of alternative processing techniques, based on the application of severe plastic deformation, where extremely high strains are imposed at relatively low temperatures without incurring any concomitant changes in the cross-sectional dimensions of the specimens. Many different SPD processing techniques have been proposed, developed and evaluated. These techniques include ECAP, high-press torsion (HPT), twist

extrusion, cylinder covered compression (CCC) and so on [43-46]. Here, one of the upgraded above methods named as ECAP used for fabricating UFG materials will be discussed in detail.

Equal channel angular pressing (ECAP) process, known also as equal-channel angular extrusion (ECAE), was first introduced by Segal and his co-workers in the 1970s and 1980s at an institute in Minsk. The basic idea was to develop a high strained metal forming process where strains may introduce into metal billets by simple shear. However, although the objective was successfully achieved, the pressing operation received only limited attention in the scientific community in the early development. This situation maintained until the 1990s when reports and overviews began to appear documenting the potential for using ECAP to produce UFG and submicrometer metals with new and unique properties [47] and these reports initiated an intense and ongoing interest in scientifically investigating, developing and ultimately utilizing the ECAP process in industrial applications. An ECAP die consists of two channels of equal cross-section interesting at an angle through which a billet of material is extruded. The billet experiences a stage of simple shear during the passing through the channel intersection [48-50]. In this sense, the name “equal channel” comes from the fact that the inlet and outlet

channels have the same cross section. This enables that the billet does not change any shape in the whole process and thus very large strain may be achieved uniformly in the bulk material by repetitive ECAP operations. The only known disadvantage of this method is that it is not continuous and requires human interference. Improvements in die design are necessary to commercialize this technology,

In summary, ECAP is one of the most efficient SPD processes capable of providing an extreme grain refinement down to the deep sub-micron range. However, the performance of an ECAP process depends sensitively on the pressing temperature. Empirically, the use of higher temperatures facilitates easier pressing and a lower propensity for crack formation in the billets. However, the achievable grain refinement and the desirable abundance of high-angle grain boundaries in an ECAP-processed materials have been shown to be reduced with increasing temperature [48, 51]. Considerable effort has therefore been put into reducing the process temperature in order to achieve more desirable microstructures, while at the same time retaining the structural integrity of billets. Very recently, Zhao et al. [52] reported the processing of Grade 2 titanium by room temperature ECAP with a channel angle of $120^{o}$ that resulted in improvement in both strength and tensile elongation of the material.

In the present work, improvement of the mechanical performance of grade 2 and grade 4 CP Ti was targeted. The variant of the ECAP process we used to obtain UFG microstructure involved encapsulation of a Ti billet in a copper case, which made it possible to conduct ECAP at a relatively low temperature of 300° C. At this temperature, grain coarsening was avoided, and a very fine grain structure was produced. The mechanical properties of titanium were raised to exceptionally high levels. In this communication we report the results of optical and transmission electron microscopy characterization of the microstructure of ECAP-modified grade 2 and grade 4 Ti, along with the computer simulation data.

## 1.2 Basic principles of equal channel angular pressing

The ECAP procedure is a metal flow process operating in simple shear and characterized by several fundamental parameters such as the strain imposed in each separate passage through the die, the slip systems operating during the pressing operation and the consequent shearing patterns presents within the as pressed billets. In generally, ECAP process is carried out by introducing a lubricated billet into a die containing two channels with equal cross-sectional area. For

sufficiently long billets, plastic flow is essentially steady and in one plane. The cannels intersect at an angle denoted by Φ near the center of the die. The process is presented in Fig. 33. Under these conditions the billet pass through the channels as rigid body, and deformation is achieved by simple shear in a thin layer of the diagonal plane at the jog of the channels. In this way the complete billet, except the small end regions and the minor surface area is deformed in the same uniform manner. The die angle determines the incremental strain intensity applied as the billet passes through the shear plane. The effective Von Misses strain per pass is following:

$$\varepsilon = \frac{2}{\sqrt{3}} cot\left(\frac{\Phi}{2}\right) \qquad (1)$$

The pressure needed to press to the billet through the punch can be determined by:

$$p = \frac{2}{\sqrt{3}} \cdot \sigma_y \cdot cot\left(\frac{\Phi}{2}\right) \qquad (2)$$

Where $\sigma_y$ is the yield stress of the material [49, 50].

In the present study the intersection channel angle is $90^{\circ}$ in order to obtain maximum strain and the billet is pressed through the die using a manual controlled hydraulic press. The plastic strain using $90^{\circ}$ was 1.16 that published by the literature [50]. Except intersection angle Φ

the curvature angle Ψ is also the important parameters to influence strain capability. Three conditions are shown in Fig.33: thus, (a) corresponds to a limiting situation where $\Psi = 0^{\circ}$, (b) corresponds to a second limiting situation where $\Psi = \pi - \Phi$ and (c) represents and intermediate condition where $0^{o} < \Psi < (\pi - \Phi)^{\circ}$, respectively. The strain is estimated by assuming a fully-lubricated specimen so that any frictional effects may be neglected.

For the situation $\Psi = 0^{\circ}$ where in Fig.34 (a), a small square element in the entrance channel, labeled *abcd*, passes through the theoretical shear plane and becomes distorted into the parallelogram labeled a'b'c'd'. I can be shown from first principles that the shear strain, γ, is given by

$$\gamma = 2\cot\left(\frac{\Phi}{2}\right) \qquad (3)$$

Using the same approach for (b) condition, it follows that

$$\gamma = \Psi \qquad (4)$$

and a similar analysis for (c) leads to the genera solution

$$\gamma = 2\cot\left(\frac{\Phi}{2} + \frac{\Psi}{2}\right) + \Psi\,\mathrm{cosec}\left(\frac{\Phi}{2} + \frac{\Psi}{2}\right) \qquad (5)$$

It follows from inspection that the general solution in Eq. (5) reduces to Eq. (3) when $\Psi = 0^{\circ}$ and to Eq. (4) when $\Psi = \pi - \Phi$. Finally, the

equivalent strain after N passes, $\varepsilon_N$, may express in a general form by the relationship [48].

$$\varepsilon_N = \frac{N}{\sqrt{3}}\left[2\cot\left(\frac{\Phi}{2}+\frac{\Psi}{2}\right)+\Psi\mathrm{cosec}\left(\frac{\Phi}{2}+\frac{\Psi}{2}\right)\right] \qquad (6)$$

Eq. (6) is consistent with an earlier estimate of the strain where a die was analyzed with $\Psi = 0^{\circ}$, with the strain after N passes as transformation Eq. (1). Thus, all of these approaches lead to similar relationships for the equivalent train but Eq. (6) has the advantage that it incorporates the angle associated with the arc of curvature, $\Psi$. Eq. (6) is also reasonably consistent with alternative approaches and it provides a simple and direct procedure for estimating the strain for any selected die having different values for $\Phi$ and $\Psi$.

The most significant advantage compare to other method is the development of near uniform, intensive and simple shear in bulk samples in a simple way. The process can easily be repeated a number of times in the same tool and very large effective deformations can be produced without changing any cross-sectional area with in different routes. The four different processing routes are presented schematically in Fig. 35 by rotating the sample. These routes contribute to different final shear patterns in the deformed

billet which crucial in dictating grain size of the refined microstructures.

Route A: In this sequence, the billet orientation is the same direction between each pass. As a result, the distortion of material element is continuously increased with each successive pass. The strongly developed laminar and fiber textures are produced via this route due to the same direction of distortion in whole part.

Rout $B_A$: The sample is deformed alternatively in two orthogonal rotations by $90^{\circ}$ between consecutive passes. In other words, the sample rotates at extrusion axis by counter clock wise $90^{\circ}$ after every odd numbered pass and clockwise $90^{o}$ after every even numbered pass.

Route $B_C$: In this condition, the sample rotates $90^{\circ}$ counter clockwise after each pass. This rough is the most efficient way in obtaining highly refined microstructures. Thus in this study route $B_C$ was chosen as processing route.

Route C: this is a hybrid route defined that is defined as two route C passes followed by a $90^{\circ}$ rotation and then additional two rout C Passes. This route produces a high amount fully worked material

and uniformly refined microstructure with a high fraction of high angle boundaries [53].

The different slip systems associated with these various processing routes which are depicted in Fig. 36 schematically where the X, Y and Z planes correspond to the three orthogonal planes and slip is shown for different passes in each processing route: thus, the planes labeled 1 through 4 correspond to the first 4 passes of ECAP. In route C, the shearing continue on the same plane in each consecutive passage through the die but the direction of shear is reversed on each pass, therefore, route C is termed as a redundant strain process and the strain is restored after every even number of passes. It is apparent that route $B_C$ is also a redundant strain process because slip in the first passes is cancelled by slip in the third pass and slip in the second pass is cancelled by slip in the fourth pass. By contrast, routes A and $B_A$ are not redundant strain processes and there are two separate shearing planes intersecting at an angle of $90^\circ$ in route A and four distinct shearing planes intersecting at angles of $120^\circ$ in route $B_A$. In routes A and $B_A$, there is a cumulative build up additional strain on each separate pass through the die.

The consequences of the distortion of these shearing systems is shown in Fig. 37 where the four major rows correspond to the four different processing routes and the illustrations depict the macroscopic distortions introduced in to a cubic elements, as viewed on the X, Y and Z planes, for up to a maximum of 8 passes through the die [54]. Therefore, for each plane of sectioning and each processing route, Fig. 37 represents the distortion visible in the faces of the cubic elements. It is evident from the figure that the cubic element is restored every 2 passes using route C and every 4 passes using route $B_C$ whereas the distortions become more acute when using routes A and $B_A$. Furthermore, there is no deformation of the cubic element on the Z plane when using routes A and C.

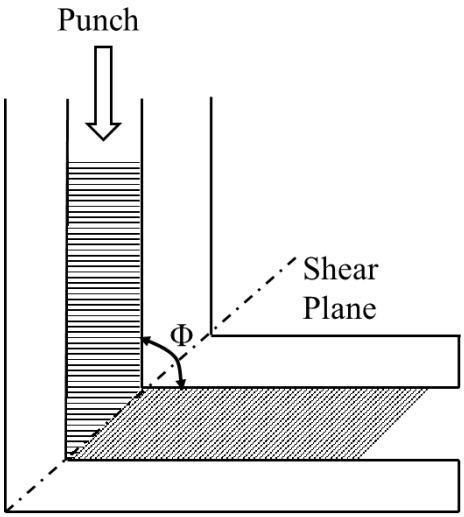


Fig. 33. Schematic diagram of describing the ECAP process. The representative materials element pass through simple shear deformation when passing the channel.

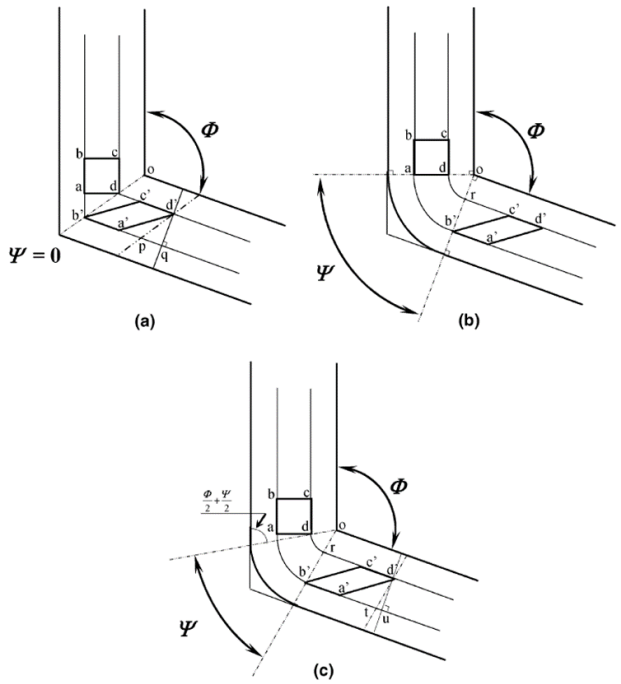


Fig. 34. Principles of ECAP where Φ is the angle of intersection of the channels and Ψ is the cornering angle of arc curvature at the point of intersection: (a) Ψ =0º (b) Ψ = π – Φ (c) and arbitrary value of Ψ lysing between Ψ = 0º and Ψ = π – Φ [48].

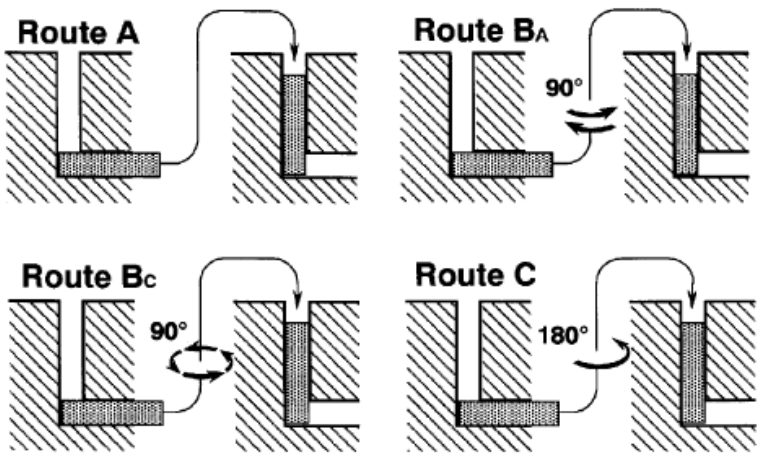


Fig. 35. Four kind of fundamental processing routes in ECAP process [48].

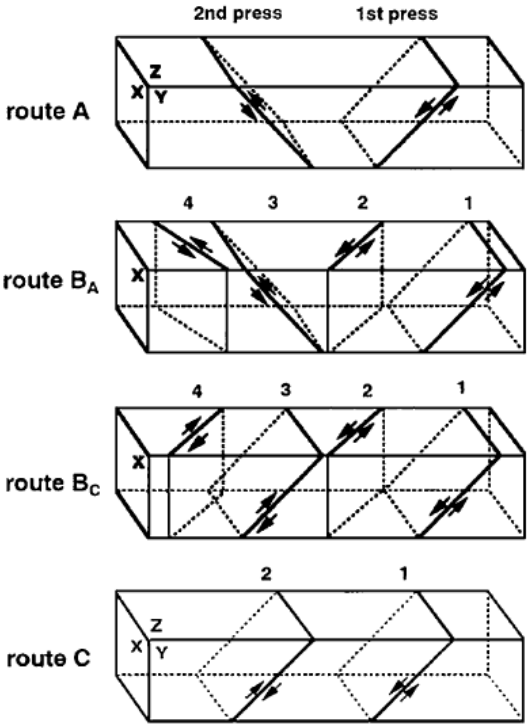


Fig. 36. The different slip systems along with the X, Y and Z planes for consecutive passes using processing routes A, $B_A$, $B_C$ and C.

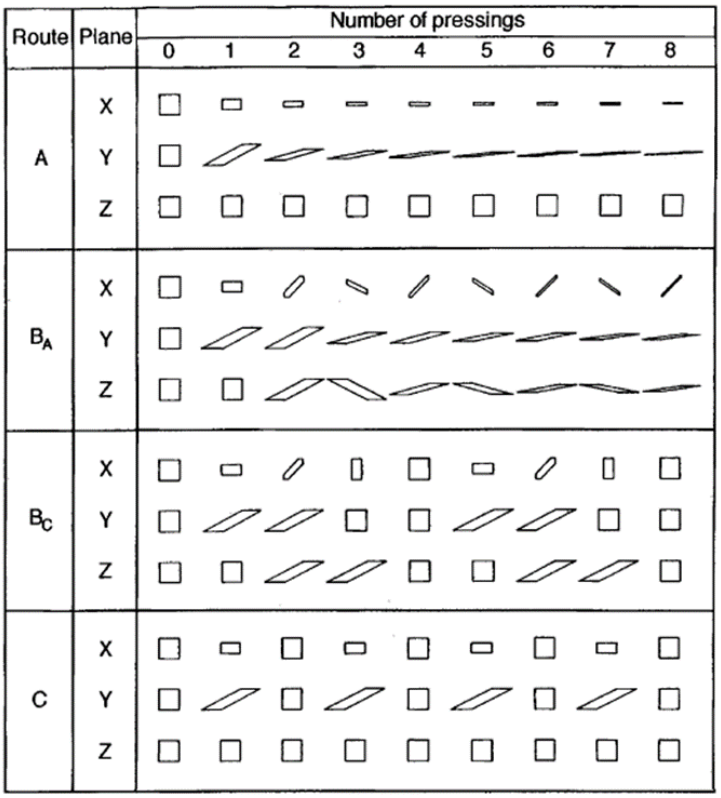


Fig. 37. The distortions introduced into cubic elements when viewed on X, Y and Z planes depending on routes A, $B_A$, $B_C$, and C when pressing through 1-8 passes.

## 2. Experiment and results

### 2.1 Materials and methods

Grade 2 and grade 4 CP titanium rods that have same chemical composition already shown in Table 1 (but different source) and microstructure distribution in Fig. 39 (a) and 41 (a) by optical microscopy were selected in the present experiments. In contrast, the samples with a diameter of 6.5 mm were cut in to billets 70 mm in length. Each billet was fully encapsulated by placing it in a copper cartridge and covered with a copper lid. A schematic diagram of such an encapsulated billet is shown in Fig. 38. ECAP of specimens encapsulated in a container has been implemented in the past [55], copper being particularly favorable as a sheath due to its good friction properties [56, 57]. Besides, encapsulation promotes uniformity of deformation of the encased billet and helps preventing cracking during the process. The outer diameter and the length of the copper cartridge were 12 mm and 80 mm, respectively. Encapsulation of a billet in copper enabled ECAP to be conducted without back-pressure at a ram speed of 1 mm/s.

The channel angle Φ is the most significant and conclusive experimental parameter because it decides the total strain imposed in

each pass, as explained in the principle of ECAP section above. Thus, it has a direct influence on the condition of the as-pressed microstructure. In the present study, the experiments were conducted using die having channel angles of $90^{\circ}$ and route $B_C$ [48] was employed in the consecutive passes in order to have the maximum strains.

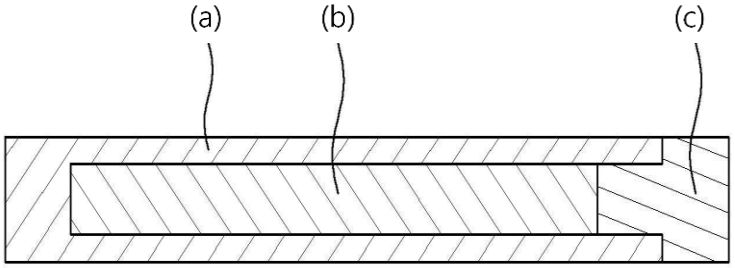


Fig. 38. Schematic diagram of an encapsulated specimen for ECAP: (a) copper cartridge; (b) titanium billet and (c) copper lid.

## 2.2 Experimental procedures

All the grade 2 and 4 titanium rods were annealed 15 minutes at 600°C before pressing in order to release residual stress and artifact defects. Then the titanium rods were encapsulated in the copper sheath and lid. In order to have lowest and optimized condition pressing temperature was decreased from 450 °C to 400 °C, 350 °C, 300 °C, and 250 °C until fracture occurs. However, all the grade 2 and grade 4 CP Ti had broken down at 250 °C. Thus, in this study the deformation temperature was chosen to be 300 °C that deformation temperature for grade 2 and grade 4 CP Ti is lower than previous studies here Ti was deformed via ECAP using 90 ° of intersection channel angle [58-60] and the all experiments mentioned below are taken at 300 °C from now on.

Depending on the above consideration, the die was preheated at 300 °C using automatically controlled heating element before pressing while the sample also heated up to 300°C using a box furnace. The heated samples pressed by route $B_C$ up to eight passes as explained above. Carbon grease was used as a lubricant during the process. After processing, specimens were naturally cooled to ambient temperature. Vickers hardness test were done as same as before in

chapter 1. Tensile tests on specimens with a gauge length of 20 mm and a diameter of 4 mm were conducted in an accordance with the ASTM E08 standard. All tensile tests were carried out at room temperature on an Instron 5586 universal testing machine using a cross-head velocity of 2 mm/min.

Microstructures were observed on cross-sections normal to the pressing direction by optical microscopy (OM) and transmission electron microscopy (TEM) using a FEI, Tecnai F20 20 microscope operating at 200 kV. The OM and TEM images taken from the normal plane of the extrude direction. Metallographic specimens were ground with SiC papers, followed by electrolytic polishing according to the procedures outlined in Ref. [61] and etching with Kroll's reagent (6% $HNO_3$, 4% HF and 90% distilled water). Thin foils for the TEM study were prepared by twin jet electro polishing using an electrolyte containing 6% perchloric acid, 35% butanol and 59% methanol [62]. EBSD also employed in order to observe microstructure characterization as well.

## 2.3 Results and discussion

### 2.3.1 Microstructure observations

The microstructures of the as-received (a), two (b), six (c) and eight (d) ECAP-processed grade 2 CP Ti are illustrated in Fig. 39. It is seen that the microstructure consists of equiaxed grains from the TEM micrograph. The average grain size, *d*, was determined from these images by the liner intercept method. The magnitude of *d* evolved from 40 μm in the initial (Fig. 39(a)) material down to 6 μm, 250 nm and eventually to 150 nm after two, six, and eight passes, respectively, whereas the microstructure of four passes had a slightly different shape of form a bi-modality was observed which is presented in Fig. 40. The possibility of those bi-modal structures will explain in the following section since the Grace 4 CP Ti also showed same tendency.

The microstructure of the as-received and the ECAP-modified grade 4 CP Ti is presented in Fig. 41. Same method was employed in order to measure the mean grain size explained above and the magnitude of *d* evolved from 16 μm in the initial (Fig. 41(a)) material down to 4 μm, 250 nm and eventually to 200 nm after, two, six and eight passes, respectively.

Note that the above grain sizes of the ECAP-processed samples are representative of most matrix grains, whilst some distinctly coarser grains that were probably retained from the original microstructure were present in the material. An apparent bi-modality of the grain structure is illustrated in the bright-field (BF) TEM micrograph in Fig. 40a and 42a for the case of four ECAP passes of grade 2 and 4 CP Ti. Under a lower magnification, the bi-modal distribution of grain size is manifested by the co-existence of regions of complex, mottled diffraction contrast (fine-grained zones) and those of relatively uniform contrast over extended areas (coarse-grained zones). While occurrence of bi-modality showed distinguishingly in the grade 4 CP Ti due to the different amount of impurity that may impede movement of dislocations during the deformation. The selected area electron diffraction (SAED) pattern recorded for a fine-grained area labeled “b” comprises continuous reflection rings, a pattern typical of ultrafine-grained structure having random grain orientations. By contrast, the pattern associated with the coarse-grained structure (area “c”) contains intense fundamental reflections resembling a major zone-axis pattern, suggesting that a significant portion of the structure is dominated by a preferred orientation.

EBSD observation was also employed in order to get clear bi-modal structure as shown in Fig. 43. Both of grade 2 (a) and grade 4 (b) CP Ti are showing combination of fine and coarse grains, especially grade 2 CP Ti shows more fractions of small and high angle boundaries than grade 4. In contrast, grade 4 has evident gap between fine and coarse grains which demonstrates that grade 2 CP Ti has faster grain refinement than grade 4 Ti. While the bi-modal structure observance already published in the early literature [42, 63-66] in an experiment of magnesium alloy. In the literature, it was explained that there is a critical grain size, *d*, and ECAP processed grain size is strongly depending on initial size of the materials. In other words, all the grains may transfer to the homogeneous fine grains until, *d*, reaches specific value in the process. However, the bi-modality of the structure dose not affects much of mechanical properties even better mechanical properties were observed. Ma [63] suggested that the large contrast in microstructural length scales associated with a bi-modal system may induce stress concentrations, where twinning activity is promoted. While the possibility of this mechanism cannot be ruled out, no evidence of twinning during uniaxial tensile tests after eight-pass ECAP processing was found in

the present study. In this approach, the bi-modal formation during the grain refinement does not influence the final product.

The texture effect does not directly incorporate in the developed model at this study during the grain refinement process. Nevertheless, it is anticipated that the model will be valid for any initial or processing routes. This general validity is anticipated because the formation of new grains along the original grain boundaries was also observed in some HCP material such as magnesium by using same process. Consistent with this approach, a recent report compared the effect of texture in an AZ31 alloy processed by rolling and ECAP and concluded that texture has no effect on the size of the newly formed grains but rather it influences the extent of these new grains and the amount of deformation required to obtain their formation [67].

Fig. 44 represents mean grain size variation of grade 2 and grade 4 CP Ti during the ECAP process. As shown in the figure, it is obvious from the curves grain size reduced dramatically from micro to nano scale. In this regards, both of grade 2 and grade 4 CP Ti had a very effective grain refinement by encapsulated ECAP process at this temperature, particularly grade 2. Depending on Hall-petch relationship between gran size and strength, it can be expected that

mechanical properties be supposed to increase than before. Furthermore, no cracks occurred during the process in both specimens.

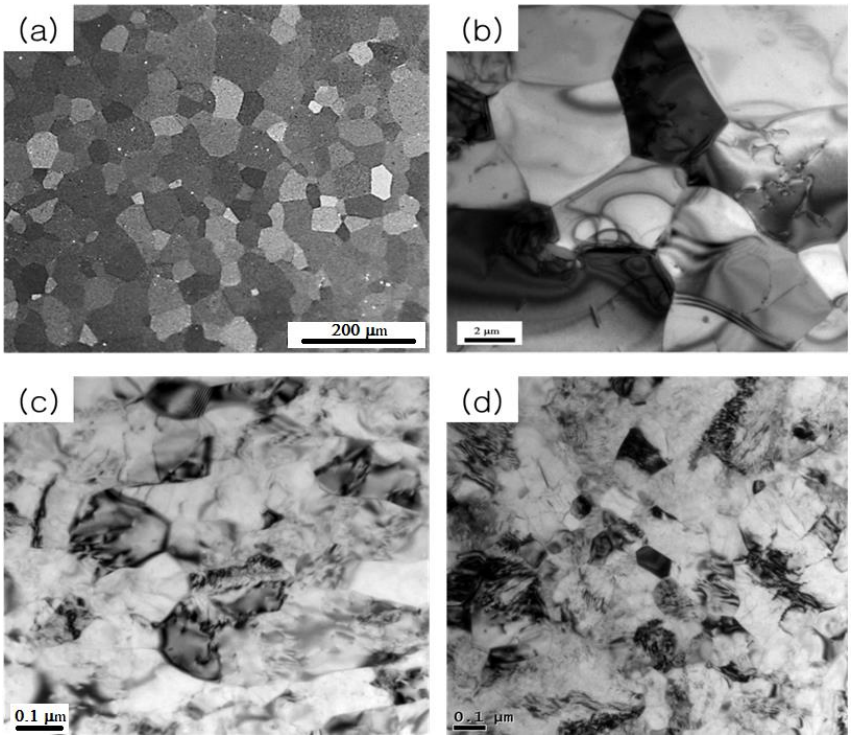


Fig. 39. Microstructure of as-received (a) and ECAP-processed CP Grade 2 Ti after two passes (b), six passes (c) and eight passes (d).

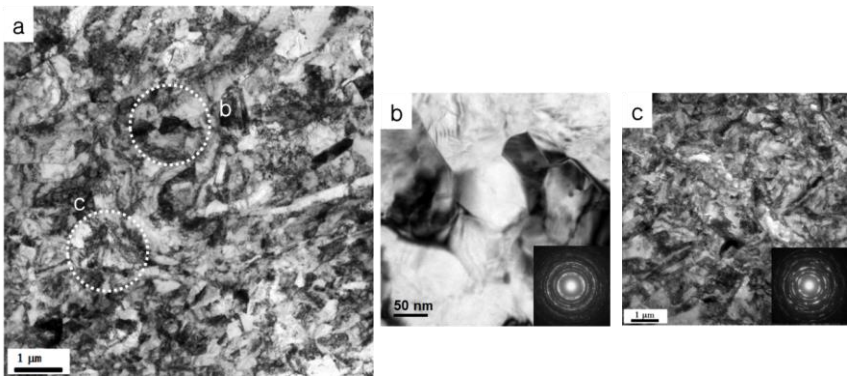


Fig. 40. BF-TEM micrograph of a specimen after four pressed Grade 2 CP Ti by ECAP showing bi-modality of grain size distribution. (b) & (c) Higher magnification images and the corresponding SAED patterns of a fine-grained and a coarse-grained zone, labeled (b) and (c) respectively, in (a). The dotted circles in (a) approximate the size of the selected area aperture used for electron diffractions.

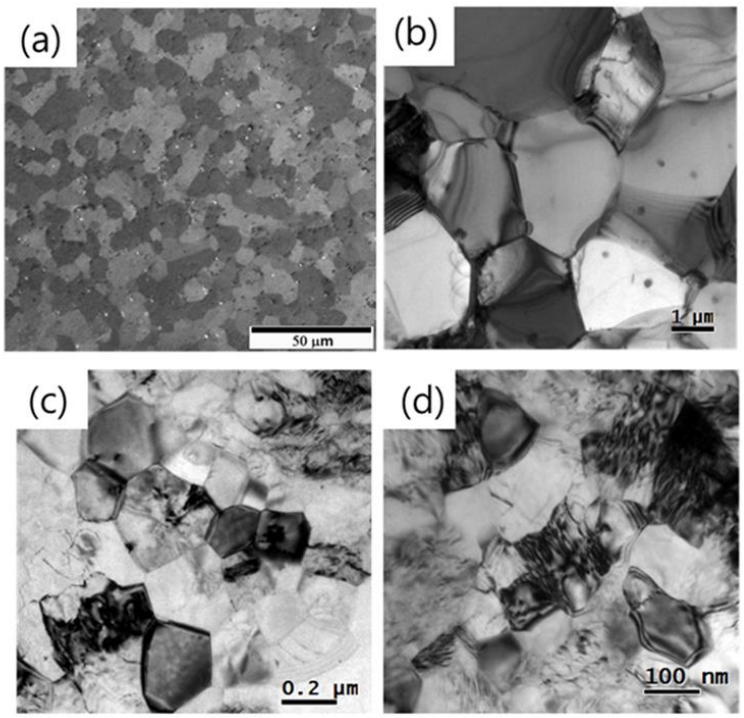


Fig. 41. Microstructure of as-received (a) and ECAP-processed CP Grade 4 Ti after two passes (b), six passes (c) and eight passes (d).

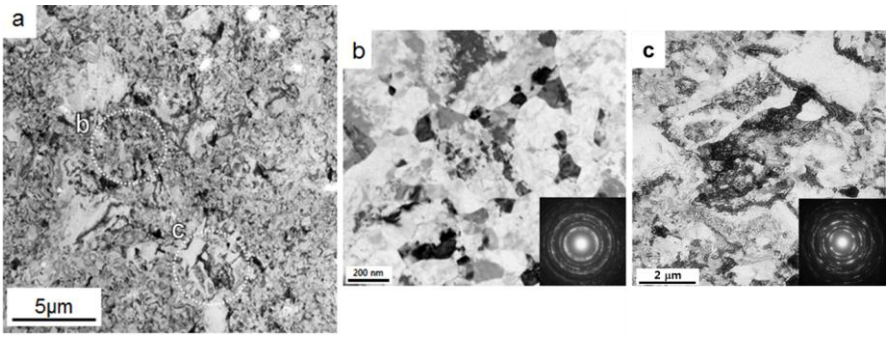


Fig. 42. BF-TEM micrograph of a specimen after four pressed Grade 4 CP Ti by ECAP showing bi-modality of grain size distribution. (b) & (c) Higher magnification images and the corresponding SAED patterns of a fine-grained and a coarse-grained zone, labeled (b) and (c) respectively, in (a). The dotted circles in (a) approximate the size of the selected area aperture used for electron diffractions.

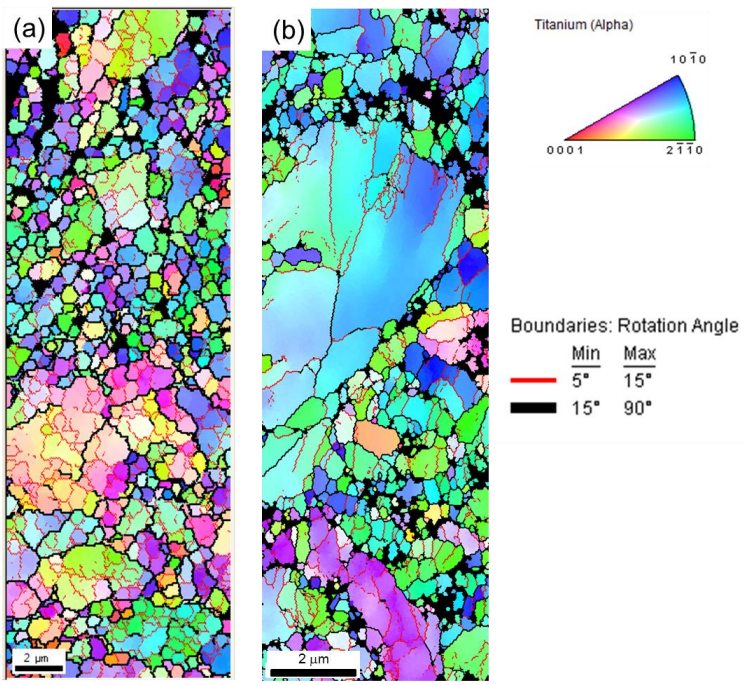


Fig. 43. EBSD microstructure of four ECAP-pressed Grade 2 (a) and Grade 4 CP Ti (b). Both micrograph shows composition coarse and fine grain where many low grain boundary misorientation angle were located inside of the coarse grains.

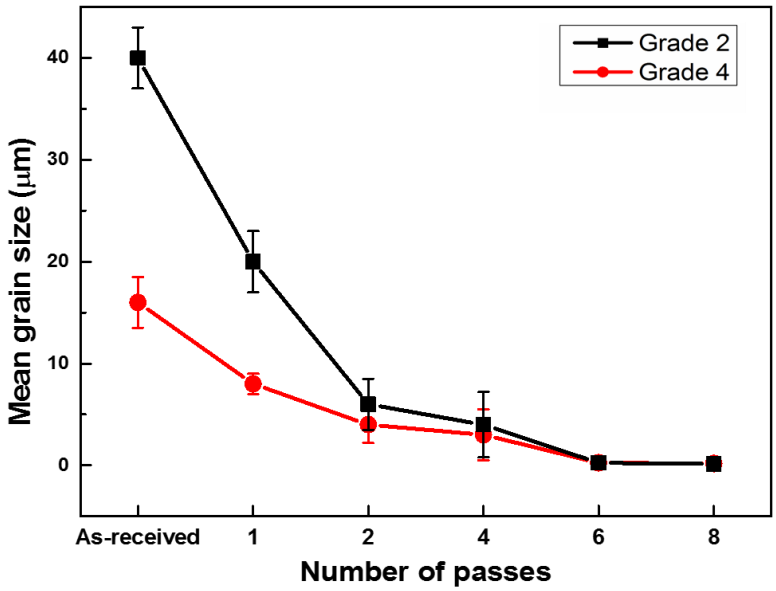


Fig. 44. Grain size variation during the ECAP process.

### 2.3.2 Mechanical properties

Fig. 45 shows the grade 2 (a) and grade 4 (b) engineering stress-strain curves of the as-received, one, two, four, six and eight ECAP processed tension specimens. As mentioned earlier all the tests were carried out on the room temperature and the specimen sere tested along the extruded direction.

It is seen that after eight passes the yield strength increased more than double of as-received grade 2 CP Ti while not losing much of fracture strain around 14% when tested along the extruded direction. In the meanwhile, after the process the yield strength enhanced about half degree in the grade 4 CP Ti while maintaining a strain around 17%. Hence, encapsulating processing could acquire exceptionally good properties both in grade 2 and grade 4 CP Ti by virtue of billet encapsulation are undoubtedly related to the increased hydrostatic pressure produced by the Cu sheath via relatively low temperature of 300°C. Finite element simulations to be reported in a follow-up chapter shows that the increase of the hydrostatic pressure during ECAP of sheathed billets is as high as about 100 MPa. This hydrostatic pressure has an effect similar to that of back-pressure, which was shown to facilitate ECAP at relatively low temperatures,

thus producing a finer grain structure and high levels of strength, cf.[68].

Fig.46 shows the Vickers hardness and ultimate tensile strength measurement results along with the number of passes. The hardness increased from 1.6 GPa to 3.0 GPa and 2.4 to 3.25 in grade 2 (a) and grade 4 (b) CP Ti, respectively. At the same time, tensile strength also enhanced from 417 MPa to 1050 MPa and 780 MPa to 1120 MPa, in which they also followed the general relationship between strength and hardness $H_V=3\sigma_{UTS.}$ In addition, these increased mechanical properties in a good agreement with grain refinement results as showed Fig. 44.

The detailed values of mechanical properties are represented in Table 4. It is a noticeable that after eight ECAP process grade 2 and grade 4 CP Ti both has over 1000 MPa of ultimate tensile strength which close to record literature values for this titanium grades and matching, or even surpassing, the levels for conventional Ti-6Al-4V alloy were obtained. While, Strengthening with the progress of ECAP due to grain refinement can be interpreted in terms of the Hall-Petch relation, $\sigma_{YS=}\sigma_{o+}k/d^{1/2}$, where $\sigma_o$ is a 'friction stress' and $k$ is the Hall-

Petch coefficient. The best fit of the data presented in Table 4 is obtained with $k \approx 0.45$ MPa/m$^{1/2}$ [7, 69].

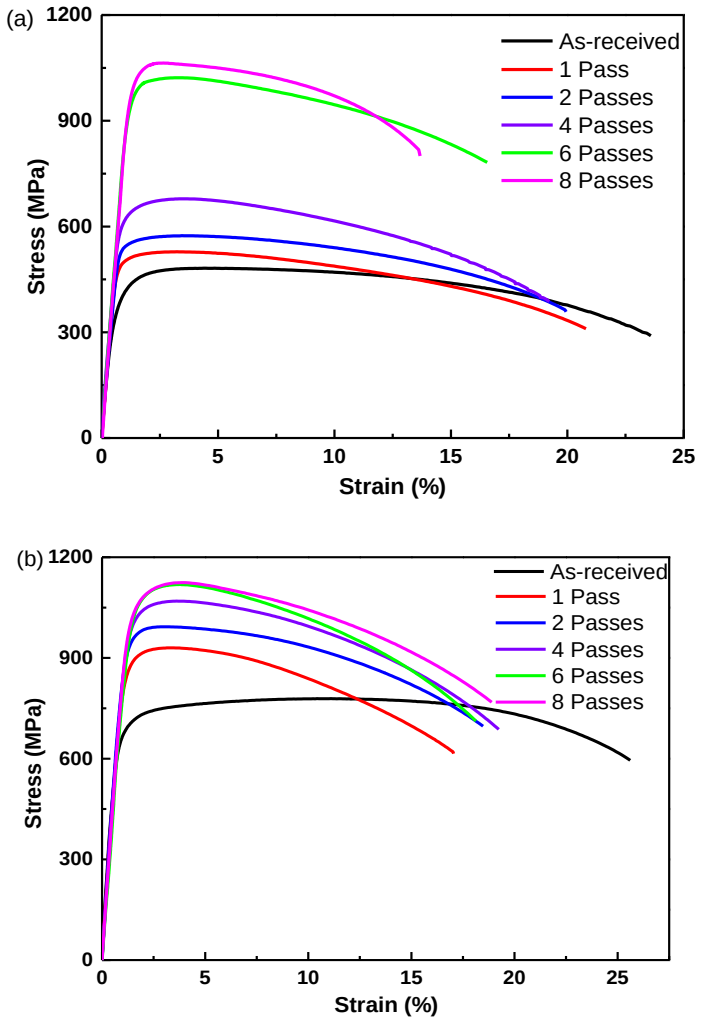


Fig. 45. Engineering stress-strain curve after 1, 2, 4, 6, and 8 ECAP-processed Grade 2 CP Ti (a) and Grade 4 CP Ti (b) along with as-received state.

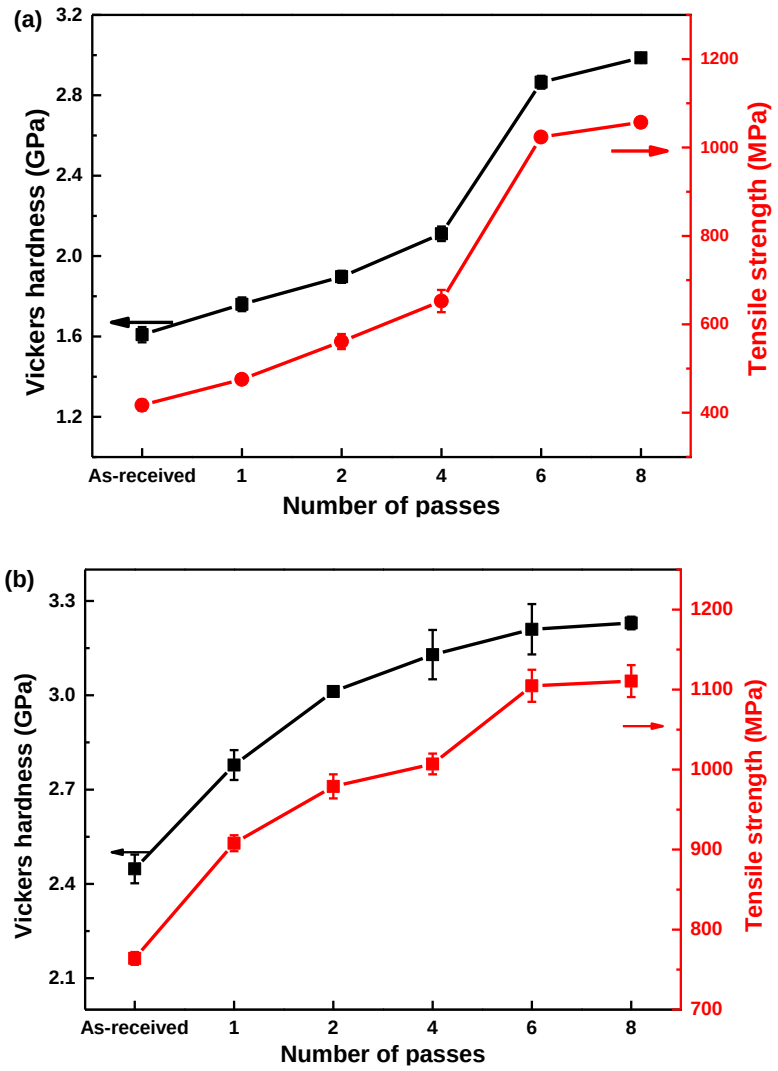


Fig. 46. Vickers hardness and ultimate tensile strength variation after ECAP process of grade 2 (a) and grade 4 (b).

Table.4. Mechanical properties of ECAP-processed CP Grade 2 and Grade 4 Ti

| Ti Grade 2 | $\sigma_{UTS}$ (MPa) | $\sigma_{YS}$ (MPa) | Elongation to break (%) | Area reduction(%) |
|---|---|---|---|---|
| As-received | 417±10 | 367 | 23.6±4 | 45 |
| 1-Passes | 475±12 | 452 | 20.8±2 | 46 |
| 2-Passes | 561±11 | 531 | 19.9±2 | 50 |
| 4-Passes | 652±12 | 610 | 19.0±3 | 52 |
| 6-Passes | 1043±21 | 916 | 16.5±2 | 55 |
| 8-Passes | 1057±20 | 1005 | 13.9±3 | 57 |

| Ti Grade 4 | $\sigma_{UTS}$ (MPa) | $\sigma_{YS}$ (MPa) | Elongation to break (%) | Area reduction(%) |
|---|---|---|---|---|
| As-received | 765±4 | 680 | 22.8±5 | 41 |
| 1-Passes | 908±10 | 872 | 15.7±2 | 43 |
| 2-Passes | 979±7 | 954 | 16.9±1 | 43 |
| 4-Passes | 1007±13 | 1002 | 17.6±2 | 50 |
| 6-Passes | 1118±20 | 1016 | 16.7±3 | 53 |
| 8-Passes | 1120±42 | 1038 | 17.3±2 | 54 |

## 2.4 Conclusions

Grade 2 and grade 4 CP titanium were successfully deformed by encapsulation-aided ECAP at a reasonably low temperature of 300 ˚C without a need for extra back-pressure. Due to the small grain size obtained (typically 150 ~ 200 nm after 8 ECAP passes), the yield strength and the ultimate tensile strength acquired values as high as 1005 MPa and 1057 MPa in grade 2 and 1038 MPa and 1120 MPa in grade 4 , respectively. In this regard, it was possible to improve the mechanical strength of pure titanium to the levels close to, or even exceeding those for the conventional Ti-6Al-4V alloys, which exhibit $\sigma_{UTS}$ values in the range from 900 MPa (annealed) to 1170 MPa (aged). Although the elongation to failure was reduced compared to that of the as received material, the overall combination of strength and ductility can be considered as being superior to that of CP Ti processed by most other SPD techniques [45, 70-73]. The values of the mechanical characteristics achieved with grade 4 titanium come close to the record values ($\sigma_{UTS}$ =1230~1250 MPa) obtained for this material by combining ECAP with further thermo mechanical processing steps [74].

## 3. FEA simulations

### 3.1 Modeling of equal channel angular pressing

Computer based FEA simulation was also conducted in order to understand encapsulation mechanism as well using same software introduced in chapter 1. But one difference is that the microstructure evolution was not included because ECAP process has same strain rate which is one of the most important advantage at this process. Thus, deformation behavior, flow stress and strain were focused and analyzed at the present simulations for getting a better understanding of the encapsulation process at low temperature.

The simulation were carried out in 3D, however, the analysis were progressed in 2D (cross-sectional view which is half plane of channel direction) due to the symmetry of the process. The schematic diagram illustrated in Fig. 47 with simulation conditions. At the present simulation, the materials formal characteristics were taken from the tensile test results at 300 ˚C as shown in (a). Furthermore, the sample were assembled as same as real experimental form that presented in (b). The total mesh of whole work piece had 10,000 numbers of elements and friction between mold and work piece set to 0.1 due to grease effect. Isothermal assumption used both of die and

work pieces in the simulation due to the constant temperature of 300°C by heating element in the real experiment and pressing speed of 1 mm/s used as well. The temperature rise was ignored during the deformation because of the low pressing speed.

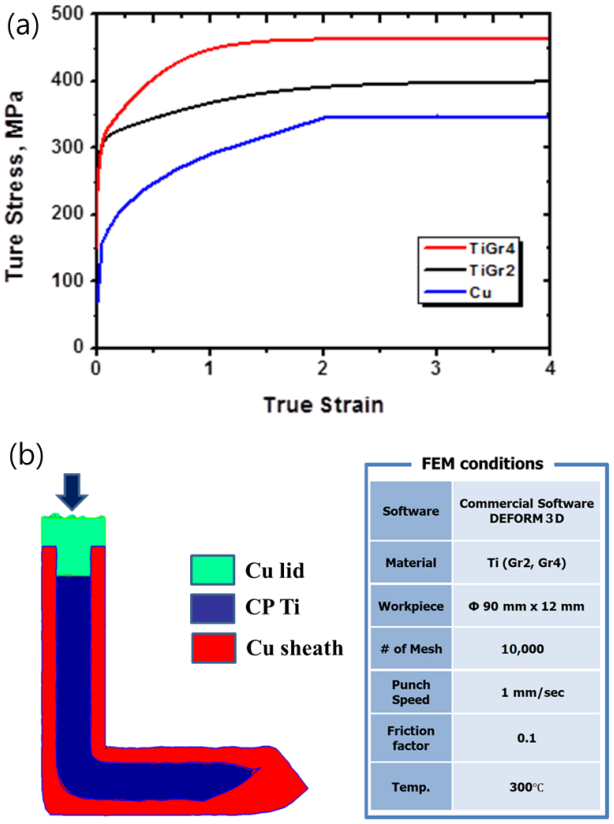


Fig. 47. Schematic diagram of true stress strain curve by experimental measurements (a) and the assembled modeling of ECAP process with the FEM conditions.

### 3.2 Results and discussions

Fig.48 illustrates the simulated shape of CP Ti samples with comparing the real experimented specimens. Both the simulated grade 2 (a) and grade 4 (b) are showed similar shape at the last step with the real specimens while grade 4 CP Ti showed more cornering gap than grade 2 due to its higher strain hardening characteristics as shown in Fig. 47(a). Fig.49 (a) shows the simulated distribution of effective stress with the distance-effective stress curve. It is evident that both grade 2 and 4 CP Ti receives uniform highest stress of 340 MPa and 440 at the cornering region which is the major deformation zone, respectively. At the same time, copper sheath receives 300 MPa of homogeneous effective stress around the titanium which means copper sheath wraps the titanium rod tightly and operates as a protection fluid during the process. The maximum shear stress were also analyzed in Fig.49 (b) along with the distance where none encapsulated condition was not show in drawing but in the diagram which showed in right side. It is evident that titanium rod receives unbalanced shear stress from bottom to upper part about 100 MPa during the pressing that would cause crack propagation to the sample in non-encapsulation condition, while encapsulated titanium has quite

uniform distribution of shear stress which is the major advantage of encapsulation and restrains crack occurrence during the deformation

The effective strain distribution of the work piece is shown in Fig.50 with the distance-effective strain curve as well. The strain induced in the titanium is nearly uniform over the entire cross-section except the front regions where in cross-ECAP the front part dose not undergoes much of deformation. According to the distance-strain graph as shown in the right side, both the grade 2 and 4 CP Ti maintained average strain value of 1.1 which is in agreement with the calculated literature value [50] during the process. In contrast, the copper sheath had relatively none homogeneous strain dispersion and even folding occurred at the bottom of front part of the specimen (arrowed part) and this results could also be found in distance-strain curves in the right side. Interestingly, front (head) part of the work piece where composed only with copper was showed same range of strain value about 0.8. In addition, the copper sheath showed higher strain value compares to the inside of the CP titanium and the strain distinction between sheath and titanium is more apparent at the grade 4 case. It demonstrates that the strain value is more closely equal when mechanical strength of the two different materials is similar; the strain value of the relatively soft material follows the strong

material's strain although there is a high strain gap in the boundaries due to the mismatch of strain hardening rate, especially at bottom part.

The distribution of mean stress by simulation, $(\sigma_x + \sigma_y + \sigma_z)/3$, was depicted in Fig.51 in order to investigate the stress state in the work piece during the ECAP process. It can be seen from the stress variable (grade 2 only analyzed due to same distribution with grade 4) depending on X, Y and Z direction shown in above that at the beginning $\sigma_y$ has highest stress due to the compressive force through the punch at the entry, but after cornering stress at three direction of X, Y and Z axis has almost equalized value $\sigma_x \approx \sigma_y \approx \sigma_z$ from the figure. Thus, it demonstrates that the stress in the inner part of the exit channel is different from that in the outer part, not only stress value, but also in the direction. The entire specimen receives including titanium rod receives compressive stress at the entry side due to the compression of the punch, and the maxima compressive stress value occurred at the inside of the cornering point. On the other hand, the passing out part of the upper area and head of the work piece (composed only with copper) in the tensile stress state since the outer part is elongated in the pressing direction, while these compressive and tensile stress would be canceled out in the cross-section (perpendicular to the passing out direction) as a consequences

of hydrostatic condition except head part. In addition, as shown in the distance-stress curve entire titanium rod receives compressive stress (minus value) in the mean stress even head part, where compressive and tensile stress existing in the boundary of titanium rod and copper sheath due to the principle of action and reaction. In this regards, it demonstrates that titanium rods maintaining the compressive stress during the whole process and head part of the copper sheath acting as a backpressure. In this consideration, it can be defined as hydrostatic-like pressure produced by the copper sheath. This hydrostatic pressure has an effect similar to that kind of back-pressure, which was shown to facilitate ECAP at relatively low temperature, thus it make possible to produce finer grain structure and high levels of strength [68].

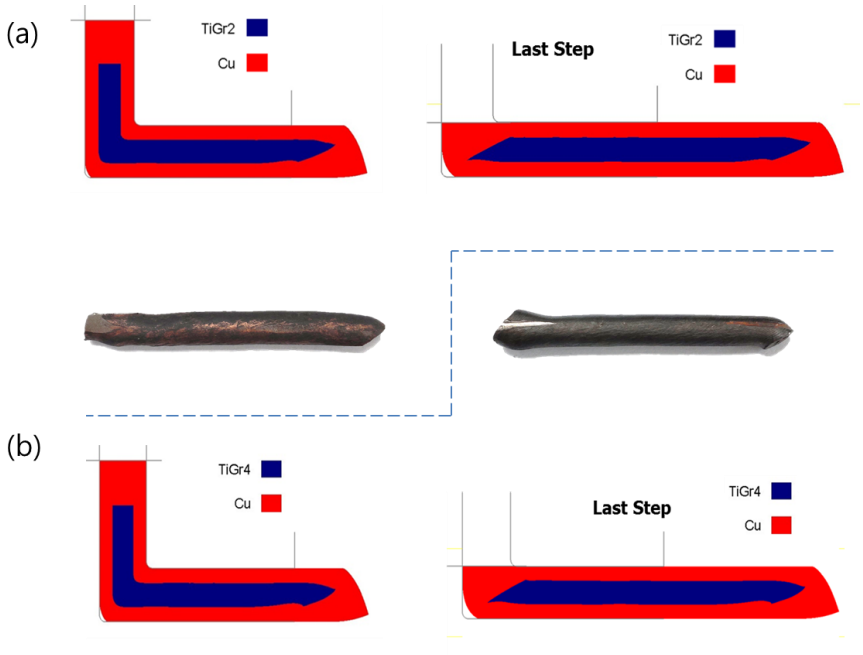


Fig. 48. Comparison of simulated Grade 2 (a) and Grade 4 (b) CP Ti after 1-ECAP processed work pieces with real specimens.

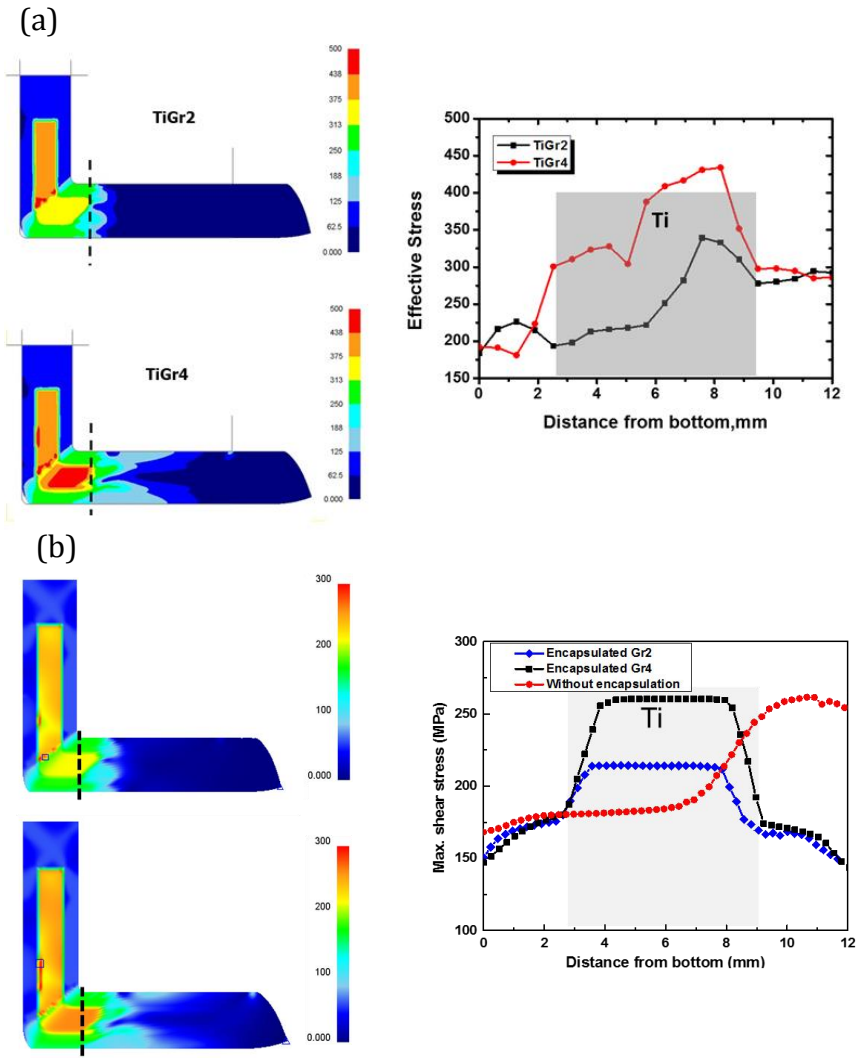


Fig. 49. Simulated effective stress variation and (a) maximum shear stress variation (b) with the diagrams of across the diameter of the work piece at different location.

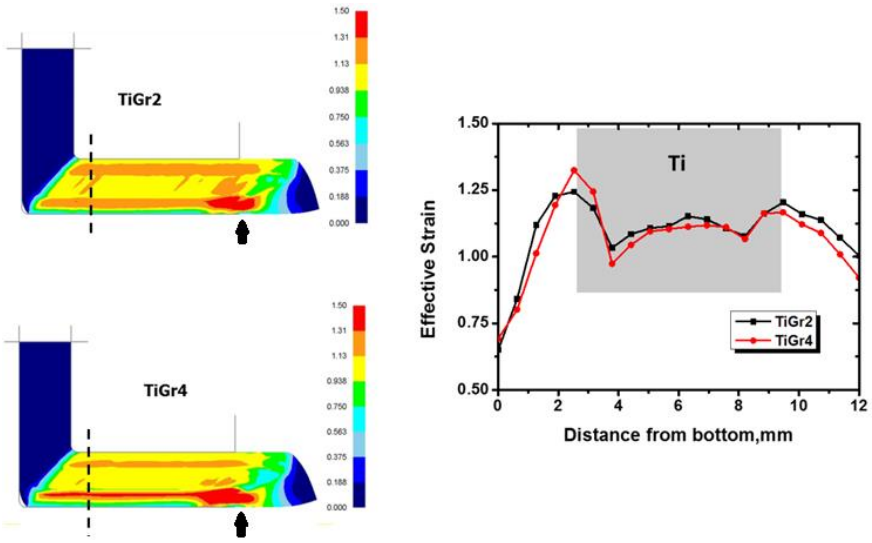


Fig. 50. Simulated effective strain variation and a diagram of across the diameter of the work piece at different location.

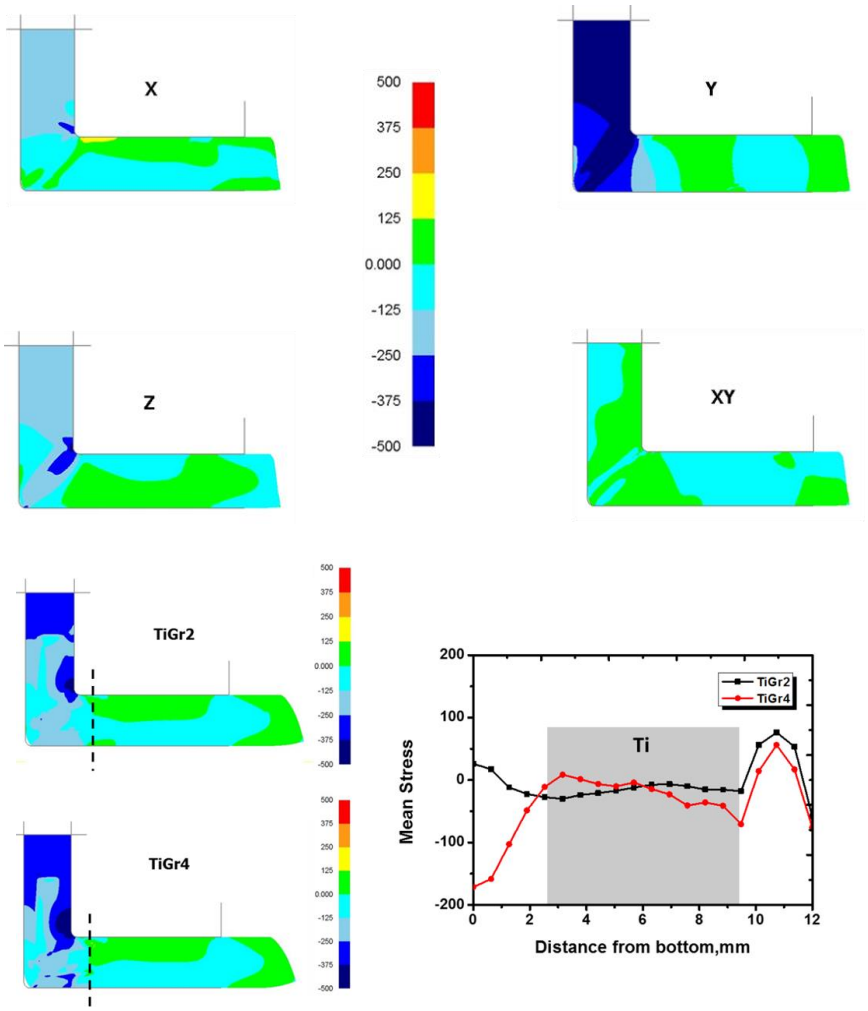


Fig. 51. Simulated mean stress variation and a diagram of across the diameter of the work piece at different location where $\sigma_{mean=} (\sigma_x + \sigma_y + \sigma_z)/3$.

### 3.3 Conclusions

A finite element analysis was developed in order to investigate the plastic deformation behavior during the encapsulated ECAP process. As expectation, the copper sheath works as a protection fluid due to the low strength and high ductility. As a result, titanium rod receives quite uniform pure shear stress during the process because the back pressure like force was activated by copper encapsulation. In addition, homogenous strain was observed in entire sample except less deformed head region because of the hydrostatic-like pressure which is in a good agreement of microstructure observation in actual experiments results.

Although the finite element modeling by using the conventional von Mises material properties results in successful outputs for the purpose, it is still has left much to be desired in the texture and dislocation evolution which is cannot be ruled out in the real ECAP process.

# Chapter Ⅲ.

# Summary and conclusions

Commercial purity grade 2 and grade 4 titanium successfully improved their mechanical properties by getting UFG structure using SPD techniques at relatively low temperature. The average grain sizes were decreased from 20 μm to 0.75 μm in grade 2 and from 16 μm to 0.77 μm in grade 4 CP Ti by decreasing the cross-sectional area of 64% using PSW process at temperature of 450 ˚C. As a result, the ultimate tensile strength increased from 378 MPa to 749 MPa in grade 2 and from 750 MPa to 926 MPa according to the Hall-petch relationship between grain size and strength. On the other hand, ECAP processed samples showed much enhanced mechanical properties than that of PSW products. In addition, homogeneous microstructure also was observed in ECAP processed specimens without changing any shape of the billets due to the equivalent strain on the entire specimen during the deformation by hydrostatic-like pressure using copper encapsulation. Accordingly, the average grain size were reduced from 40 μm to 150 nm in grade 2 and from 16 μm to 200 nm, while ultimate strength increased from 417 MPa to 1057 MPa and from 765 MPa to 1120 MPa, correspondingly to each grade 2 and 4 CP Ti at temperature of 300˚C.

In both PSW and ECAP processed grade 2 CP Ti showed dramatic improvement on strength as exceeding double value of than

that of initial state. In contrast, grade 4 CP Ti only increased 24% and 46% by PSW and ECAP respectively. However, these enhanced values are sufficient for previous literature recorded values [45, 70-73] in which further thermomechanical processing steps were required after deformation. The strategy of enhanced strength that SPD process was based on ECAP combination with extrusion, rolling, or drawing in UFG grade 2 and grade 4 titanium are illustrated in Fig. 52 [52, 70, 75-82]. Although the maximum strength did not reach to the highest record it has advantage that no additional treating was applied in the present study, especially in ECAP process.

The FEA simulations were successfully conducted and compared with real experimental results. Both the PSW and ECAP processes showed expected trends in effective stress and strain state compare to the real condition. Although microstructure evolution based simulation has an insufficient results due to the limitation of the software it is still enough to be deduced from the stress and strain distribution for understanding the trend of microstructure evolution. In contrast, ECAP simulation results showed more reliable results compare to the real state, even if texture and dislocation reaction did not count in the simulation.

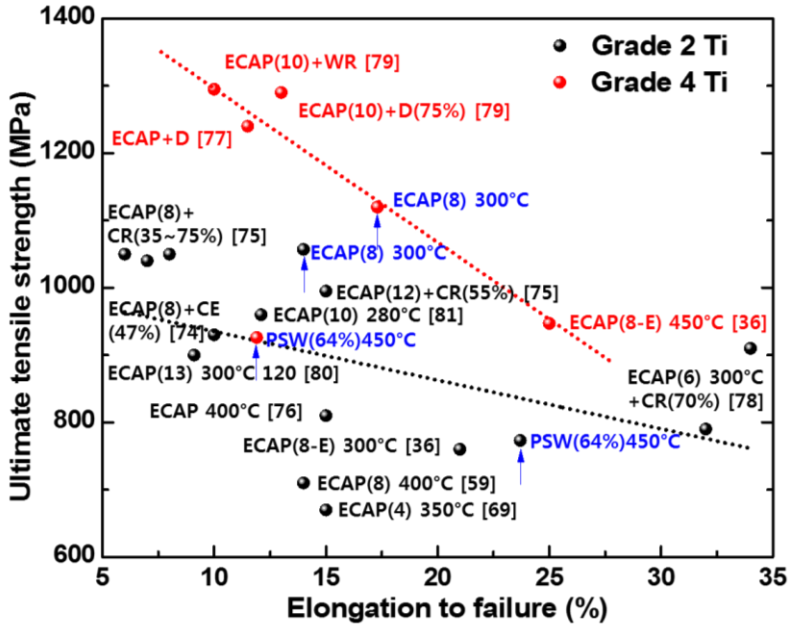


Fig. 52. The correlation of the elongation to failure and the ultimate tensile strength for CP Ti in previous conventional and UFG states.

# 초 록

입자 크기가 작아지면 재료의 강도가 증진되는 관계를 이용하여 재료로 하여금 우수한 기계적 물성을 갖도록 재 탄생 시키는 연구가 지난 수십여 년 동안 진행되어왔다. 극한소성변형은 이중에서도 티타늄 및 티타늄합금과 같은 변형이 어려운 재료를 효과적으로 소성변형을 유도함으로써 재료의 기계적 물성을 증진할 수 있는 것으로 잘 알려져 있다. 본 논문에서는 유성압연과 등통로각 압축 두 가지 극한소성방법을 저온에서 이용하여 기존의 고온에서만 (0.5Tm 보다 높은 온도) 진행할 수 있는 단점을 극복하여 보다 더 효율적으로 재료의 입자 미세화에 성공하였다. 현재 가벼우면서도 높은 강도를 이유로 시중에서 우주항공분야이거나 생체재료 분야에서 가장 많이 사용되고 있는 순수 티타늄 그레이드 2 와 4 을 주 재료로 선택하여서 연구를 진행하였다. 과거에도 많은 연구들이 순수티타늄을 극한소성변형을 유도하여 초미세립을 갖는 재료로 재탄생 시키는데 중점을 두고 진행되어왔지만 티타늄 재료와 같이 HCP 구조를 갖는 재료의 고질적인 문제로 인하여 실험공정에서의 온도나 속도와 같은 많은 부분을 희생시켜야만 했다. 하지만 본 논문에서는 상용 순수 티타늄에 맞는 최적의 온도를 찾아내어 고질적인 단점을 해결 함으로써 기존의 공정에 비하여 한층 더 업그레이드 된 방법으로 티타늄의 기계적 물성을 극대화 시켰다.

이렇게 얻은 티타늄의 기계적 물성은 고강도 티타늄 합금에 버금가거나 심지어 초과하기까지 하였다. 또한 컴퓨터를 이용한 시뮬레이션을 통하여 새로운 공정이 성공할 수 있었던 이유를 밝혀내고 실제 실험결과와 비교를 하여 실험 메커니즘을 알아내었다.

**주요어:** 순수 티타늄, 유성압연, 등통로각 압축, 극한소성변형, 초미세립, 기계적 물성.

**학 번:** 2009-30892

## References

[1] Zhang XW. Numercical simulation and experimental research of three-roll helical rolling. 2011.

[2] Shih CK, Hung CH. Experimental and numerical analyses on three-roll planetary rolling process. Journal of Materials Processing Technology. 2003;142:702-9.

[3] De X. Principles of three roll planetary rolling. 1988;3:4.

[4] Gao HY, Wang, J G. Applications and research of 76 PSW. 1997;16:3.

[5] Zou SP. Applications and development of three roll planetary rolling. 1982;2.

[6] Salem AA, Kalidindi SR, Semiatin SL. Strain hardening due to deformation twinning in alpha-titanium: Constitutive relations and crystal-plasticity modeling. Acta Materialia. 2005;53:3495-502.

[7] Salem AA, Kalidindi SR, Doherty RD, Semiatin SL. Strain hardening due to deformation twinning in alpha-titanium: Mechanisms. Metallurgical and Materials Transactions a-Physical Metallurgy and Materials Science. 2006;37A:259-68.

[8] Lopatin NV. Microstructure evolution in pure titanium during warm deformation by combined rolling processes. Materials Science

and Engineering a-Structural Materials Properties Microstructure and Processing. 2012;556:704-15.

[9] Li B, Zhang SH, Zhang HQ, Zhang GL. Microstructure and properties of copper tube during three-roll planetary rolling. Journal of Materials Engineering and Performance. 2008;17:499-505.

[10] Li B, Zhang SH, Zhang GL, Zhang HQ. Prediction of 3-D temperature field of TP2 copper tubes in three-roll planetary rolling process. Journal of Materials Processing Technology. 2008;205:370-5.

[11] Kim SHP, E.S. ; Kim, H.J. ; Bae, J.C. ; Huh, M.Y. . Evolution of Strain States and Microstructures During Three-roll Screw Rolling of Copper Rods. Transactions of Materials Processing. 2008;17:4.

[12] Marc Andre Meyers KKC. Mechanical behavior of materials. 2 ed: Cambridge University Press; 2008.

[13] M.J. Tan XJZ. Dynamic recrystallization in commercially pure titanium. Journal of Achievements in Materials and Manufacturing Engineering. 2006;18.

[14] M.J. Tan XJZ. Microstructure evolution of CP titanium during high temperature deformation. AMSE. 2007;28:5-11.

[15] Salem AA, Kalidindi SR, Doherty RD. Strain hardening of titanium: role of deformation twinning. Acta Materialia. 2003;51:4225-37.

[16] Yang Y, Wang BF. Dynamic recrystallization in adiabatic shear band in alpha-titanium. Materials Letters. 2006;60:2198-202.

[17] Xu F, Zhang XY, Ni HT, Cheng YM, Zhu YT, Liu Q. Effect of twinning on microstructure and texture evolutions of pure Ti during dynamic plastic deformation. Materials Science and Engineering a-Structural Materials Properties Microstructure and Processing. 2013;564:22-33.

[18] William F. Smith JH. Foundations of materials science and engineering. 4 ed2006.

[19] Shewchuk. JR. An Introduction to the Conjugate Gradient Method Without the Agonizing Pain. 1.25 ed. School of Computer Science Carnegie Mellon University: Pittsburgh; 1994.

[20] Lv LP. Finite element method and application in forging engineering. Northwestern Polytechnical University1989.

[21] Wang JS. Applications and technology of finite element method of plastic deformation in metal: Metallurgy and instustrial 2003.

[22] 金属塑性成形仿真技术: 上海交通大学出版社; 1999.

[23] Wu SJ, Hwang YM, Chang MH. A three-dimensional finite element analysis of the three-roll planetary mill. Journal of Materials Processing Technology. 2002;123:336-45.

[24] Shih CK, Hung CH, Hsu RQ. The finite element analysis on planetary rolling process. Journal of Materials Processing Technology. 2001;113:115-23.

[25] Allwood JM, Utsunomiya H. A survey of flexible forming processes in Japan. Int J Mach Tool Manu. 2006;46:1939-60.

[26] Lee JKK, K. W. ; Cho, H. Y. FEA of Pipe Rolling Process Using Planetary Rolling Mill for Stainless Steel. Journal of the Korean Society of Marine Engineering. 2011;35:244-51.

[27] Lee DN, Han HN. Recrystallization Textures of Metals and Alloys2013.

[28] Kratochvil J. Mechanism of Grain Refinement Induced by Severe Plastic Deformation. Materials Science Forum. 2011;667-669:5.

[29] Guo-Zheng Q. Characterization for Dynamic Recrystallization Kinetics Based on Stress-Strain Curves2013.

[30] Gourdet S, Montheillet F. A model of continuous dynamic recrystallization. Acta Materialia. 2003;51:2685-99.

[31] Mironov S. Yu. SGA, Zherebtsov S.V. Microstructure and texture evolution during continuous dynamic recrystallization at warm deformation of titanium. Materials Science Forum. 2004;467-470:1211-6.

[32] Zarkades A, Larson, F.E. Experimental Determination of Texture and Mechanical Anisotropy of Tensile Properties in Commercially Pure Titanium Sheet. AMMRC TR 67-05. 1967.

[33] Suwas S, Beausir B, Toth LS, Fundenberger JJ, Gottstein G. Texture evolution in commercially pure titanium after warm equal channel angular extrusion. Acta Materialia. 2011;59:1121-33.

[34] Valiev RZ IR, Alexandrov IV. Bulk Nanostructured Materials from Severe Plastic Deformation. Progress in Materials Science. 2000;45:103.

[35] Valiev RZ, Estrin Y, Horita Z, Langdon TG, Zehetbauer MJ, Zhu YT. Producing bulk ultrafine-grained materials by severe plastic deformation. Jom-Us. 2006;58:33-9.

[36] Valiev R. Nanostructuring of metals by severe plastic deformation for advanced properties. Nat Mater. 2004;3:511-6.

[37] Purcek G, Yapici GG, Karaman I, Maier HJ. Effect of commercial purity levels on the mechanical properties of ultrafine-

grained titanium. Materials Science and Engineering a-Structural Materials Properties Microstructure and Processing. 2011;528:2303-8.

[38] Ivanov M, Kolobov Y, Golosov E, Kuz'menko I, Veinov V, Nechaenko D, et al. Mechanical properties of mass-produced nanostructured titanium. Nanotechnologies in Russia. 2011;6:370-8.

[39] Zhao YH, Zhu YT, Lavernia EJ. Strategies for Improving Tensile Ductility of Bulk Nanostructured Materials. Advanced Engineering Materials. 2010;12:769-78.

[40] Semenova IP, Valiev RZ, Yakushina EB, Salimgareeva GH, Lowe TC. Strength and fatigue properties enhancement in ultrafine-grained Ti produced by severe plastic deformation. Journal of Materials Science. 2008;43:7354-9.

[41] Krasilnikov N, Lojkowski W, Pakiela Z, Valiev R. Tensile strength and ductility of ultra-fine-grained nickel processed by severe plastic deformation. Materials Science and Engineering a-Structural Materials Properties Microstructure and Processing. 2005;397:330-7.

[42] Wang YM, Chen MW, Zhou FH, Ma E. High tensile ductility in a nanostructured metal. Nature. 2002;419:912-5.

[43] Valiev RZ, Korznikov AV, Mulyukov RR. Structure and Properties of Ultrafine-Grained Materials Produced by Severe

Plastic-Deformation. Materials Science and Engineering a-Structural Materials Properties Microstructure and Processing. 1993;168:141-8.

[44] Valiev RZ. Structure and mechanical properties of ultrafine-grained metals. Materials Science and Engineering a-Structural Materials Properties Microstructure and Processing. 1997;234:59-66.

[45] Yang XR, Zhao XC, Fu WJ. Deformed Microstructures and Mechanical Properties of CP-Ti Processed by Multi-Pass ECAP at Room Temperature. Rare Metal Materials and Engineering. 2009;38:955-7.

[46] Xu C, Xia KN, Langdon TG. Processing of a magnesium alloy by equal-channel angular pressing using a back-pressure. Materials Science and Engineering a-Structural Materials Properties Microstructure and Processing. 2009;527:205-11.

[47] Valiev RZ, Krasilnikov NA, Tsenev NK. Plastic-Deformation of Alloys with Submicron-Grained Structure. Materials Science and Engineering a-Structural Materials Properties Microstructure and Processing. 1991;137:35-40.

[48] Valiev RZ, Langdon TG. Principles of equal-channel angular pressing as a processing tool for grain refinement. Progress in Materials Science. 2006;51:881-981.

[49] Segal VM. Equal channel angular extrusion: from macromechanics to structure formation. Materials Science and Engineering a-Structural Materials Properties Microstructure and Processing. 1999;271:322-33.

[50] Segal VM. Materials Processing by Simple Shear. Materials Science and Engineering a-Structural Materials Properties Microstructure and Processing. 1995;197:157-64.

[51] Shin DH, Kim I, Kim J, Lee CS, Hwang SK. Effects of equal channel angular pressing temperature on deformation structures of pure Ti. Materials Science and Engineering a-Structural Materials Properties Microstructure and Processing. 2003;342:302-10.

[52] Zhao XC, Yang XR, Liu XY, Wang XY, Langdon TG. The processing of pure titanium through multiple passes of ECAP at room temperature. Materials Science and Engineering a-Structural Materials Properties Microstructure and Processing. 2010;527:6335-9.

[53] Barber RE, Dudo T, Yasskin PB, Hartwig KT. Product yield for ECAE processing. Scripta Materialia. 2004;51:373-7.

[54] Valiev RZ. Recent developments of SPD processing for fabrication of bulk nanostructured materials. Thermec'2003, Pts 1-5. 2003;426-4:237-44.

[55] Cornwell LR, Hartwig KT, Goforth RE, Semiatin SL. The equal channel angular extrusion process for materials processing. Materials Characterization. 1996;37:295-300.

[56] Zebardast M, Taheri AK. The cold welding of copper to aluminum using equal channel angular extrusion (ECAE) process. Journal of Materials Processing Technology. 2011;211:1034-43.

[57] Quang P, Jeong YG, Hong SH, Kim HS. Equal channel angular pressing of carbon nanotube reinforced metal matrix nanocomposites. Key Engineering Materials. 2006;326-328 I:325-8.

[58] Zhu YT, Kolobov YR, Grabovetskaya GP, Stolyarov VV, Girsova NV, Valiev RZ. Microstructures and mechanical properties of ultrafine-grained Ti foil processed by equal-channel angular pressing and cold rolling. Journal of Materials Research. 2003;18:1011-6.

[59] Stolyarov VV, Zhu YT, Alexandrov IV, Lowe TC, Valiev RZ. Grain refinement and properties of pure Ti processed by warm ECAP and cold rolling. Materials Science and Engineering a-Structural Materials Properties Microstructure and Processing. 2003;343:43-50.

[60] Stolyarov VV, Zhu YT, Lowe TC, Valiev RZ. Microstructure and properties of pure Ti processed by ECAP and cold extrusion.

Materials Science and Engineering a-Structural Materials Properties Microstructure and Processing. 2001;303:82-9.

[61] Chen CC, Chen JH, Chao CG, Say WC. Electrochemical characteristics of surface of titanium formed by electrolytic polishing and anodizing. Journal of Materials Science. 2005;40:4053-9.

[62] Shin DH, Kim I, Kim J, Kim YS, Semiatin SL. Microstructure development during equal-channel angular pressing of titanium. Acta Materialia. 2003;51:983-96.

[63] Ma E. Eight routes to improve the tensile ductility of bulk nanostructured metals and alloys. JOM Journal of the Minerals, Metals and Materials Society. 2006;58:49-53.

[64] Lopovok R, Estrin Y, Popov MV, Langdon TG. Enhanced superplasticity in a magnesium alloy processed by equal-channel angular pressing with a back-pressure. Advanced Engineering Materials. 2008;10:429-33.

[65] Liu Y, Zhou J, Hui D. A strain-gradient plasticity theory of bimodal nanocrystalline materials with composite structure. Composites Part B: Engineering. 2012;43:249-54.

[66] Figueiredo RB, Langdon TG. Grain refinement and mechanical behavior of a magnesium alloy processed by ECAP. Journal of Materials Science. 2010;45:4827-36.

[67] del Valle JA, Ruano OA. Influence of texture on dynamic recrystallization and deformation mechanisms in rolled or ECAPed AZ31 magnesium alloy. Materials Science and Engineering a-Structural Materials Properties Microstructure and Processing. 2008;487:473-80.

[68] Estrin Y, Kim HE, Lapovok R, Ng HP, Jo JH. Mechanical Strength and Biocompatibility of Ultrafine-Grained Commercial Purity Titanium. Biomed Res Int. 2013.

[69] Salem AA, Kalidindi SR, Doherty RD. Strain hardening regimes and microstructure evolution during large strain compression of high purity titanium. Scripta Materialia. 2002;46:419-23.

[70] Ko YG, Shin DH, Park KT, Lee CS. An analysis of the strain hardening behavior of ultra-fine grain pure titanium. Scripta Materialia. 2006;54:1785-9.

[71] Furukawa M, Horita Z, Langdon TG. Factors influencing the shearing patterns in equal-channel angular pressing. Materials Science and Engineering a-Structural Materials Properties Microstructure and Processing. 2002;332:97-109.

[72] Raab GI, Polyakov AV, Gunderov DV, Valiev RZ. Formation of a nanostructure and properties of titanium rods during equal-channel

angular pressing CONFORM followed by drawing. Russian Metallurgy (Metally). 2010;2009:416-20.

[73] Islamgaliev R, Kazyhanov V, Shestakova L, Sharafutdinov A, Valiev R. Microstructure and mechanical properties of titanium (Grade 4) processed by high-pressure torsion. Materials Science and Engineering: A. 2008;493:190-4.

[74] Semenova I, Valiev R, Yakushina E, Salimgareeva G, Lowe T. Strength and fatigue properties enhancement in ultrafine-grained Ti produced by severe plastic deformation. Journal of Materials Science. 2008;43:7354-9.

[75] Zhu YT, Stolyarov VV, Lowe TC, Valiev RZ. Microstructure and properties of pure Ti processed by ECAP and cold extrusion. Materials Science and Engineering a-Structural Materials Properties Microstructure and Processing. 2001;303:82-9.

[76] Zhu YT, Stolyarov VV, Alexandrov IV, Lowe TC, Valiev RZ. Grain refinement and properties of pure Ti processed by warm ECAP and cold rolling. Materials Science and Engineering a-Structural Materials Properties Microstructure and Processing. 2003;343:43-50.

[77] Vinogradov AY, Stolyarov VV, Hashimoto S, Valiev RZ. Cyclic behavior of ultrafine-grain titanium produced by severe plastic

deformation. Materials Science and Engineering a-Structural Materials Properties Microstructure and Processing. 2001;318:163-73.

[78] Valiev RZ, Semenova IP, Latysh VV, Rack H, Lowe TC, Petruzelka J, et al. Nanostructured titanium for biomedical applications. Advanced Engineering Materials. 2008;10:B15-B7.

[79] Sordi VL, Ferrante M, Kawasaki M, Langdon TG. Microstructure and tensile strength of grade 2 titanium processed by equal-channel angular pressing and by rolling. Journal of Materials Science. 2012;47:7870-6.

[80] Semenova IP, Polyakov AV, Raab GI, Lowe TC, Valiev RZ. Enhanced fatigue properties of ultrafine-grained Ti rods processed by ECAP-Conform. Journal of Materials Science. 2012;47:7777-81.

[81] Raab GI, Soshnikova EP, Valiev RZ. Influence of temperature and hydrostatic pressure during equal-channel angular pressing on the microstructure of commercial-purity Ti. Materials Science and Engineering a-Structural Materials Properties Microstructure and Processing. 2004;387:674-7.

[82] M. Greger MW, L. Kander. Mechanical properties of ultra-fine grain titanium. Journal of Achievements in Materials and Manufacturing Engineering. 2010;40:33-40.

# Acknowledgement

XRD 가 먼지도 모르고 무작정 달려들어 공부를 시작한지가 엊그제 같은데 벌써 졸업이라는 시간을 맞이하게 되었네요. 멀리만 느껴졌던 졸업을 정작 앞두고 나니 마음 한구석이 시원섭섭하게 아려오는 듯싶습니다.

저를 낳아주시고 키워주시고 어려운 상황에서도 항상 뒤에서 아낌없이 지지해주신 부모님께 우선 감사의 마음을 전하고 싶습니다. 어릴 적 공부를 하고 싶어도 못한 원한을 저한테 기대하고 싶은 마음을 이제 풀어드렸다고 생각하니 기쁘기 그지없습니다. 부모님에 대한 감사의 글을 단 몇 글자에 적을 수는 없지만 “감사합니다”는 말로 표현하고 싶습니다.

다음으로 저를 이 자리까지 올 수 있게 도와주신 박순자 교수님과 저의 지도교수님이신 김현이 교수님께 감사의 말씀을 올리고 싶습니다. 한번의 스승은 영원한 스승이라는 말씀을 가슴 깊이 새겨있겠습니다. 많은 기회와 기대를 주심에도 불구하고 항상 교수님의 기대에 충분히 부응하지 못한 저 자신을 되돌려보니 부끄러울 따름입니다. 아직도 부족한 저 자신이지만 교수님께서 보여주신 인품과 연구에 대한 열정을 저의 남은 인생까지 명심하여 저 자신을 항상 채찍질 하겠습니다. 그리고 바쁜 와중에도 저의

박사논문 심사를 해주신 서울대 한흥남 교수님, 박은수 교수님 그리고 고려대 고영학 교수님 진심으로 감사 드립니다. 또한 연구실 선배님이시자 고향 선배님이신 이용호 교수님께도 큰 감사의 인사를 드립니다.

지난 6 년반 동안 가족보다 더 가족처럼 동고애락을 같이한 SLIM 식구들 정말 고마웠습니다. 지금은 졸업을 하시고 자신의 분야를 개척해나가고 계시는 선배 박사님들이 아무것도 모르는 후배를 가르쳐 주시느라고 정말로 수고가 많으셨습니다. 또한 선배들을 잘 따라주고 어려운 부탁도 잘 들어주는 후배님들도 너무 고마웠습니다. 한동안 즐거웠던 SLIM 모토멤버들인 지훈이형, 창훈이형, 봉규형, 철민, 현도 그리고 장태식과의 행복한 시간도 이젠 추억으로 남게 되었습니다. 이제 곧 학위를 시작하는 신입생들 호용, 현, 광희, 병석 그리고 다영이 앞으로 진행되는 모든 실험과 일들이 잘 풀리길 기원하며 해마다 좋은 성과가 있기를 진심으로 기원합니다.

이어서 유학생활을 함께 해온 친구들이자 대학동창인 박영훈, 변명철, 김영걸, 황병춘 그리고 유학준비 같이 하면서 1 년동안 함께 조교를 해온 변명선 모두 진심으로 고맙고 힘들 때나 좋은 일 있을 때나 서로 생각해주고 함께 웃고 떠들던 시간이 너무나 소중하고 앞으로도 우리의 우정이 영원하길 바란다.

끝으로 함께 유학 생활하면서 항상 옆에서 챙겨주고 남편을 따라주며 게다가 저한테 보배 같은 아들 승윤이까지 낳아주고 키우느라고 고생이 많았지만 한번도 불평을 하지 않는 저의 아내한테 사랑한다고 말하고 싶습니다. 그리고 우리 복덩이 승윤이는 앞으로 아무런 탈 없이 건강하게 잘 자라길 바라며 감사의 글을 마칩니다.

제가 이름을 적지 않았다 하여 감사의 마음이 부족한 것이 아니고 오히려 너무나 많은 고마운 분들의 도움을 받은 것에 비하면 결코 종이 한 장에 표현을 할 수 없음을 알기에 항상 감사의 마음을 갖고 살아가겠으며 부디 지켜봐 주시길 바랍니다.

I hereby want to give a special thanks to Professor Yuri Estrin. Thank you for your kind and nice tutoring on my research and your support was greatly helpful.

2014 년 02 월

리 원 룡 올림